Cylindrical confinement of semiflexible polymers

Pablo Vázquez-Montejo, Zachary McDargh, Markus Deserno, and Jemal Guven

P

Cylindrical confinement of semiflexible polymers

Pablo Vázquez-Montejo,[1, *] Zachary McDargh,[1, †] Markus Deserno,[1, ‡] and Jemal Guven[2, §]

[1]Department of Physics, Carnegie Mellon University,
5000 Forbes Ave, Pittsburgh, PA 15213, USA
[2]Instituto de Ciencias Nucleares, Universidad Nacional Autónoma de México
Apdo. Postal 70-543, 04510 México, DF, MÉXICO

Equilibrium states of a closed semiflexible polymer binding to a cylinder are described. This may be either by confinement or by constriction. Closed completely bound states are labeled by two integers, the number of oscillations, n, and the number of times it winds the cylinder, p, the latter a topological invariant. We examine the behavior of these states as the length of the loop is increased by evaluating the energy, the conserved axial torque and the contact force. The ground state for a given p is the state with $n = 1$; a short loop with $p = 1$ is an elliptic deformation of a parallel circle; as its length increases it elongates along the cylinder axis, with two hairpin ends. Excited states with $n \geq 2$ and $p = 1$ posses n-fold axial symmetry. Short (long) loops possess energies $\approx pE_0$ (nE_0), with E_0 the energy of a circular loop with same radius as the cylinder; in long loops the axial torque vanishes. Confined bound excited states are initially unstable; however, above a critical length each n-fold state becomes stable: the folded hairpin cannot be unfolded. The ground state for each p is also initially unstable with respect to deformations rotating the loop off the surface into the interior. A closed planar elastic curve aligned along the cylinder axis making contact with the cylinder on its two sides is identified as the ground state of a confined loop. Exterior bound states behave very differently, if free to unbind, as signaled by the reversal in the sign of the contact force. If $p = 1$, all such states are unstable. If $p \geq 2$, however, a topological obstruction to complete unbinding exists. If the loop is short, the bound state with $p = 2$ and $n = 1$ provides a stable constriction of the cylinder, partially unbinding as the length is increased. This motif could be relevant to an understanding of the process of membrane fission mediated by dynamin rings.

I. INTRODUCTION

The confinement of semi-flexible polymers or filaments by curved surfaces is increasingly recognized to be a key element in a number of physical processes. The best studied examples are presented in biology: DNA, actin filaments, and microtubules, for instance, have persistence lengths of $50\,\text{nm}$ [1], $\sim 16\,\mu\text{m}$ [2] and several millimeters [3], respectively. Because such polymers need to navigate an intracellular environment crowded by membranes and proteins, over and over again one needs to understand how they interact with these structures. DNA in eukaryotic cells, for instance, makes a virtue of necessity, wrapping around the core of cylindrical histones to facilitate their condensation [4–6]; intermediate filaments (such as spectrins or lamins) may adsorb onto membranes and, in the process, modify their elastic properties [7–9]; membrane fission is also frequently driven by the polymerization of tightly winding stiff filaments of the protein dynamin, whose winding around the neck of a nascent vesicle is believed to cut the vesicle from its parent membrane [10–12]. Since in these and other examples the persistence length can be quite a bit larger than the radii of curvature to which these polymers are confined, it is a good approximation to ignore additional thermal fluctuations and focus on ground state solutions, which is what we will do in this paper. The opposite limit, confining highly flexible filaments, is a classical topic in polymer science, which is reviewed in Ref. [13]. While stiff filaments are especially frequent and well studied in the context of biology, they also occur in other situations, and confinement issues arise there, too. For instance, single walled carbon nanotubes have a diameter dependent persistence length in the tens of micrometer range [14], and their adsorption onto surfaces or their interplay with other mesoscopic microstructures is currently a subject of considerable interest for engineers as well as physicists [15, 16].

———————

*[*]pablov@andrew.cmu.edu
[†]zmcdargh@andrew.cmu.edu
[‡]deserno@andrew.cmu.edu
[§]jemal@nucleares.unam.mx*

The defining feature of semi-flexibility is that the polymer's persistence length substantially exceeds molecular scales, such as the monomer size or thickness. This is physically important, because it means that the energetics of bending decouples from the minutiae of the chemical structure and can thus be described to very good accuracy by a continuum-elastic Hamiltonian depending largely on geometry. The simplest such energy functional describes a semi-flexible polymer as a one-dimensional smooth space-curve and quadratically penalizes its Frenet curvature, $\kappa(s)$ [17–20]:

$$H_{\mathrm{B}} = \frac{A}{2} \int \mathrm{d}s \; \kappa(s)^2 \; , \tag{1}$$

where s is the arc length along the curve, and A is the bending rigidity. Since there are no other energy terms competing with the bending, from now on we set the bending rigidity to unity, $A = 1$. A functional variation $\delta H_{\mathrm{B}} = 0$ leads to the Euler-Lagrange (EL) equations which characterize the solutions that minimize this energy.

Substantially more complicated functionals are not only conceivable but have also been studied, adding for instance stretching, twisting [21–23], spontaneous curvature [24] or the higher derivative Frenet torsion [25]. An environmental bias may imply a separate dependence on the geodesic and normal curvatures, or even the geodesic torsion [26]. For the purpose of this paper we restrict our attention to the elementary energy, Eq. (1). The problem is still non-trivial because the energy needs to be amended with the constraint confining the space-curve to the surface. One needs to accommodate this constraint in the calculus of variations, as described for example in [27]. We will only consider the limiting case in which the surface is much stiffer than the polymer itself, so that the shape of the surface remains unaffected. The opposite limit, in which the polymer is infinitely rigid and the surface adjusts, has recently been studied by Božič et al. [28], who considered a circular ring constricting an axisymmetric neck. Of course, in many physically relevant situations both the polymer and the surface respond to each other's presence. However, the discussion of two elastic objects of different dimensionalities pitting their forces against each other through a mutually confining geometric constraint is a long story which will have to await a future treatment.

The first general discussion of surface-constrained elastic curves à la Eq. (1) was given by Nickerson and Manning [29, 30], who derived the Euler-Lagrange (EL) equation for this constrained minimization problem. As an application, they studied cylindrical confinement with a particular choice of boundary conditions [30]. Later, Marky and Manning considered the wrapping of DNA around a histone octamer taking into account an adhesive interaction between the polymer and its substrate [31]. More recently, the problem was treated by van der Heijden, who also included a twist degree of freedom on isotropic [32] and anisotropic [33] rods with forces applied at the boundaries. Later still, van der Heijden et al. [34] studied self-contacts of a cylindrically confined elastic rod. In this work, the elastic curve is treated as a Kirchhoff-rod or more generally within the context of Cosserat theory. We will follow the strategy introduced by two of the authors in Ref. [27], where the surface constraint was enforced using a local Lagrange multiplier in the variational principle, which can be identified as the external source of stresses to which the polymer is subject due to the confinement. This provides direct access to the magnitude of the confining forces as well as their sign which will vary along the polymer. Formally, the multiplier is identified with the normal projection of the derivative of the force vector, which permits one to quantify the loss of Euclidean invariance of the constrained system. In this approach it is unnecessary to assume any constitutive relations between the bending moments, the energy density and the strains: the balance of forces and torques follow from the minimization of the energy; these two vectors are also identified. For simplicity we will restrict our attention to closed polymer loops.

The equilibrium shapes of semiflexible polymer loops, modeled as elastic curves, confined by a sphere were examined in some detail in Ref. [27], (see Refs. [35, 36] for a more physical and realistic treatment, involving numerical analysis, see also [37, 38] for a detailed study of the dynamics of confined semiflexible polymers employing simulations, as well as [39, 40] addressing the effect of electrostatics on the adsorption of polymers rings onto surfaces with spherical and cylindrical geometry.). The analytical treatment in Ref. [27] was facilitated by identifying the three conserved quantities—corresponding to the three components of the torque—associated with the spherical symmetry. The EL equations could be integrated completely in terms of elliptic functions. It was shown that the physics of these states depends very sensitively on the length of the loop. Indeed, the ground state itself alternated between two states as the length was increased. The forces transmitted to the sphere was also shown to depend both non-monotonically and discontinuously on this length. As the length becomes increasingly large, all bound states tend increasingly towards geodesic behavior. The aim of the present paper is to investigate systematically the binding of a semi-flexible polymer loop to a cylinder, not only by its confinement within it but also by the forced constriction of the cylinder by an exterior loop. In the absence of additional adhesive forces the latter has no analogue on a sphere.

A cylinder is distinguished from a sphere both geometrically (curvature anisotropy) and topologically. Specifically it is non-compact. Each of these features will play a role: some times alone, other times together with unexpected outcomes.

We begin by showing how the conservation laws associated with the residual Euclidean symmetries conspire not only to yield a quadrature, but also to provide the appropriate observables for characterizing the underlying physics. While we lose rotational symmetry about the local surface normal, the underlying axial and translational symmetry still provide two conservation laws, one for the axial torque and another for the axial force. These first integrals are each of third order in derivatives of the embedding functions. However, the two can be combined into a single equation eliminating one derivative, which can be cast as a simple quadrature in terms of the tangent angle. This quadrature involves three parameters, the two conserved quantities as well as a Lagrange multiplier associated with the fixed length of the polymer.

We are particularly interested in how the equilibrium states, and in particular candidate ground states depend on the length of the loop. For a given length, such loops will be characterized uniquely by two integers, the number of times the loop wraps around the cylinder, p, and the number of oscillations it executes in the process (its dihedral symmetry of order n). These states differ from their spherical counterparts, also labeled by two integers, in a number of ways. If its length is small, the loop does not yet explore the non-compact direction; the reduced symmetry however identifies the bound ground state as an elliptical deformation of a circular loop (with $n = 1$, see Fig. 1(a)), a state without any equilibrium counterpart on a sphere. As the length increases the loop elongates along the cylinder axis terminating in two hairpin ends. At some point, as we will show, the loop self-intersects, thereafter scissoring–in accordion fashion–along the axial direction. States with higher dihedral symmetries are unstable initially (a state with $n = 2$ is illustrated in Fig. 1(b)). As the length is increased, however, these excited states also grow along the non-compact direction, forming folded hairpins. And once they develop, it costs energy to undo these folds. The important point is that beyond some critical length, the folded state become snagged energetically on the cylinder; they are stabilized. There is no analogous process for loops binding to a sphere. Also, unlike a sphere where states morph periodically into multiple coverings of a geodesic circle with increasing loop length, the hairpins that develop diverge increasingly from geodesic behavior, while at the same time tending towards a simple characteristic structure. Indeed the asymptotic energy assumes the remarkably simple form, $E_{p,n} \to nE_0$, independent of p, where E_0 is the energy of a circular loop with a radius equal to that of the cylinder. It is independent of the topology, so that the energy of these limit states is highly degenerate. We will describe in detail how the axial torque, the energy and, perhaps most importantly, the forces responsible for confinement depend on the length of the loop for each pair of integers, n and p. The direction of the normal force transmitted to the surface obviously depends on which side the
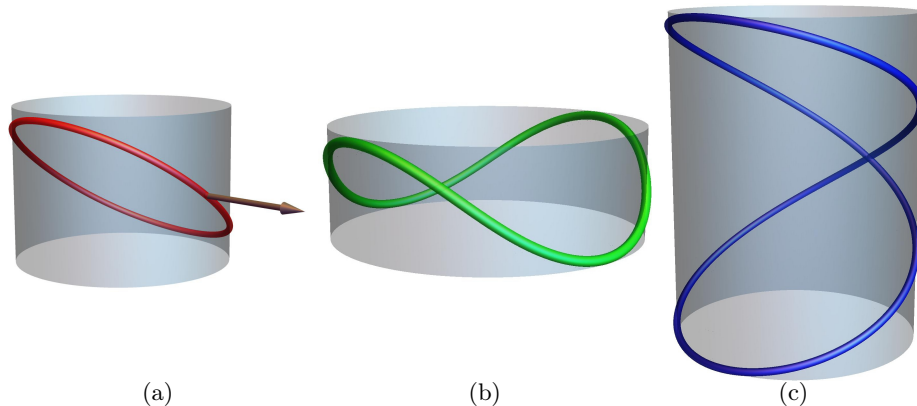

FIG. 1: (Color online) (a) Elliptic state with $n = 1$ and $p = 1$. (b) Two-fold state with $n = 2$ and $p = 1$. (c) Folded eight-figure state, $n = 1$ and $p = 2$. The arrow indicates the local normal vector to the surface, which signifies the direction along which confining forces have to act in order to keep the polymer on the surface, with a sign convention further discussed in the text.

polymer is bound to: when the loop is inside, positive (negative) values represents outward (inward) forces. If the loop is outside, these sign conventions are reversed. The latter are especially interesting because, as we will show, an external polymer may constrict the cylinder, a happy conspiracy permitted by the topology, an impossibility on a sphere. While in the spherical case the confining force on an interior bound loop always pushes it up against the sphere, we will see that for cylinders the sign of the confining force generally changes along equilibrium bound states. This would indicate that additional forces are required to stabilize the state (deriving for instance from an adhesion energy) if it is free to unbind. In the case of interior bound states, we find that the offending regions are extremely localized in the neighborhood of hairpins, suggesting that the state is stabilized if the loop simply takes a shortcut off the surface so as avoids these regions. If the reader feels uncomfortable taking shortcuts, they may assume that

an additional constant sticky force is provided where necessary. We will also provide an exact description of states confined within the cylinder making partial contact with its walls. The corresponding ground state is a planar loop aligned along the cylinder axis making contact on its two sides: a vertical safety pin. This state has lower energy than its bound counterpart. In the absence of additional adhesive forces, the bound interior ground state–if sufficiently short–is expected to be unstable with respect to deformation into the cylinder rotating it into this state. As its length increases, however, it would appear to turn stable with respect to such deformations, protected by an ever-increasing energy barrier. A bound exterior state winding the cylinder once ($p = 1$) would, on the other hand, simply peel off relaxing towards a circular loop. If the loop winds twice or more times around the cylinder (see Fig. 1(c)), however, this is no longer the case.[1] A figure of eight possesses a lower energy than a free doubly-wound circular loop, and would be expected to remain completely attached to the cylinder if the loop is sufficiently short. Longer loops will not be completely attached but they would nevertheless be expected to embrace the cylinder at least partially, applying a force at the points where they remain in contact. This is because the presence of the cylinder obstructs their passage to a singly-wound circular loop. The existence of such a motif might be relevant to the constriction of membrane necks, indicating as it does that topology may facilitate the constriction process.

The axial torque also depends in a surprisingly non-trivial way on the length of the loop. It vanishes as this length become increasing large in all equilibrium loops. However it does not do so monotonically: we discover the existence of intriguing non-trivial states in which the axial torque vanishes which occur when the length is tuned appropriately. These states admit an analytic description.

The paper is organized as follows: In section II, we develop the general framework for axially symmetric binding. The first integral of the Euler-Lagrange (EL) equation, associated with rotational symmetry, is derived in (II A). This framework is applied specifically to the cylinder in Sect. (III). The equilibrium states of a closed curve are constructed in Sect. IV. The axial torques, the energies, and the forces they transmit to the surface are determined. This is done perturbatively for loop states approximating a multiply-covered circle and numerically otherwise. We end with a discussion and a few suggestions for future work in Section V. A number of useful identities and derivations are collected in a set of appendices where the analysis of vertical confined loops, loops with vanishing axial torque and force, and the comparison of elastic curves on the cylinder with their planar counterparts are also presented.

II.   CURVES CONSTRAINED TO SURFACES

Consider a space curve in Euclidean space $\mathbb{E}^3$, $\Gamma : s \to \mathbf{Y}(s)$ parametrized by arc-length constrained to lie on a surface Σ. This surface is described in parametric form by the mapping $\Sigma : (u^1, u^2) \to \mathbf{X}(u^1, u^2) \in \mathbb{E}^3$. The tangent vectors adapted to this parametrization are $\mathbf{e}_a = \partial \mathbf{X}/\partial u^a$, $a = 1, 2$, the unit vector normal to the surface is $\mathbf{n}$, the induced surface metric is $g_{ab} = \mathbf{e}_a \cdot \mathbf{e}_b$ and the extrinsic curvature tensor is $K_{ab} = \mathbf{e}_a \cdot \partial_b \mathbf{n}$. The confined curve can then also be described as a surface curve $\Gamma_\Sigma : s \to (U^1(s), U^2(s))$. The surface-bound curve also carries a Darboux frame, $\{\mathbf{T}, \mathbf{l}, \mathbf{n}\}$, where $\mathbf{T} = \mathbf{Y}'$ is the unit tangent vector to Γ,[2] $\mathbf{n}(U(s))$ is the restriction of the unit normal vector along the curve, and $\mathbf{l} = \mathbf{n} \times \mathbf{T}$ is the conormal tangent to the surface, that is, the vector normal to the curve Γ but tangent to the surface. The structure equations–analogous to the Frenet-Serret (FS) equations–describing how the Darboux frame rotates along the curve, are given by [41]

$$\mathbf{T}' = \kappa_g \mathbf{l} - \kappa_n \mathbf{n}, \quad \mathbf{l}' = -\kappa_g \mathbf{T} + \tau_g \mathbf{n}, \quad \mathbf{n}' = \kappa_n \mathbf{T} - \tau_g \mathbf{l}, \tag{2}$$

where the geodesic and normal curvatures, κ_g and κ_n, as well as the geodesic torsion τ_g, are defined by

$$\kappa_g = \mathbf{T}' \cdot \mathbf{l} = l^a t^b \nabla_b t_a, \qquad \kappa_n = -\mathbf{T}' \cdot \mathbf{n} = t^a t^b K_{ab}, \qquad \tau_g = \mathbf{l}' \cdot \mathbf{n} = -t^a l^b K_{ab}. \tag{3}$$

Here t^a and l^a are the components of the vectors $\mathbf{T}$ and $\mathbf{l}$ with respect to the surface tangent basis $\mathbf{e}_a$, $a = 1, 2$: $\mathbf{T} = t^a \mathbf{e}_a$, $\mathbf{l} = l^a \mathbf{e}_a$. ∇_a is the covariant derivative compatible with g_{ab}. Whereas κ_n and τ_g depend on the extrinsic curvature; κ_g is defined intrinsically, it depends only on the surface metric g_{ab}. The FS frame is related to its Darboux counterpart through a rotation by an angle ω about the tangent direction. This connection between the two frames provides a decomposition of the FS curvatures into its intrinsic and extrinsic parts

$$\kappa_g = \kappa \cos\omega, \quad \kappa_n = \kappa \sin\omega, \quad \tau = \tau_g - \omega', \tag{4}$$

---

[1] Note that a short interior bound figure of eight would be expected to unwind into the confined planar vertical hairpin state

[2] Here, and elsewhere, prime represents derivation with respect to the arc-length s.

so that $\kappa^2 = \kappa_g^2 + \kappa_n^2$. The torsion τ is given by the difference between the geodesic torsion and ω', the rotation rate of one frame with respect to the other. Note that τ_g involves two derivatives whereas τ involves three. The extra derivative is associated with the derivative of ω.

In equilibrium, one finds that the tension along the curves is balanced by a normal force due to the confinement by the surface [26, 27]

$$\mathbf{F}' = -\lambda \mathbf{n}, \tag{5}$$

where the tension in the loop $\mathbf{F}$ is given by

$$\mathbf{F} = \left(\frac{\kappa_g^2 + \kappa_n^2}{2} - C\right)\mathbf{T} + \left(\kappa_g' + \kappa_n \tau_g\right)\mathbf{l} - \left(\kappa_n' - \kappa_g \tau_g\right)\mathbf{n}. \tag{6}$$

$\mathbf{F}$ represents the tension on a curve segment exerted by the segment with lower value of arclength [25], for instance, for a spiral traversed upwards, it provides the force exerted on a segment by the region below. The constant C is associated with the constraint of fixed length and can be identified with the Hamiltonian [26].

The tangential Euler-Lagrange derivative $\varepsilon_{\mathbf{T}} = \mathbf{F}' \cdot \mathbf{T}$ vanishes identically, a consequence of the fact that the only relevant degrees of freedom are geometrical.

The projection of Eq. (5) onto $\mathbf{l}$ provides the EL equation

$$\varepsilon_{\mathbf{l}} = \mathbf{F}' \cdot \mathbf{l} = \kappa_g'' + \kappa_g \left(\frac{\kappa_g^2 + \kappa_n^2}{2} - \tau_g^2 - C\right) + \frac{\left(\kappa_n^2 \tau_g\right)'}{\kappa_n} = 0. \tag{7}$$

This equation was first derived in reference [30] using a procedure different from that in [27]. Note that it involves the two curvatures as well as the geodesic torsion. In general, the curve will not follow a geodesic with $\kappa_g = 0$.

The corresponding projection onto $\mathbf{n}$ determines the magnitude of the force λ transmitted to the surface

$$\lambda = -\mathbf{F}' \cdot \mathbf{n} = \kappa_n'' + \kappa_n \left(\frac{\kappa_g^2 + \kappa_n^2}{2} - \tau_g^2 - C\right) - \frac{\left(\kappa_g^2 \tau_g\right)'}{\kappa_g}. \tag{8}$$

Thus the normal force is completely determined when the local geometry is known. Its magnitude will vary along the contact region even for confinement by a sphere. For a curve confined inside the surface, when λ is positive (negative) the curve is pushing (pulling) the surface. This expression is missing in the framework presented in [30]. It was presented in [27].

A. Axial symmetry and residual conserved torques

The integrability of the EL equations for the unconstrained curve is a consequence of the Euclidean invariance of its energy, which implies the conservation of both forces and torques. The constrained counterpart will not be integrable, for there will not be a sufficient number of conserved quantities; in general, under confinement, one surrenders not only translational invariance, but also rotational invariance. The torque about the origin per unit length of the curve, $\mathbf{M}$, is given by two contributions, the torque due to the force $\mathbf{F}$ about the curve's position and an intrinsic torque

$$\mathbf{M} = \mathbf{Y} \times \mathbf{F} + \mathbf{S}, \quad \text{where} \quad \mathbf{S} = \kappa_g \mathbf{n} - \kappa_n \mathbf{l}. \tag{9}$$

Like the tension vector $\mathbf{F}$, the vector $\mathbf{M}$ provides the torque on a curve segment exerted by the one with a lower value of s. For a free curve the torque vector is conserved, $\mathbf{M}' = 0$, which can be cast in the manifestly translational invariant form $\mathbf{T} \times \mathbf{F} + \mathbf{S}' = 0$ [25]. By contrast, for a confined curve one has instead

$$\mathbf{M}' = \varepsilon_{\mathbf{l}} \left(\mathbf{Y} \times \mathbf{l}\right) - \lambda \left(\mathbf{Y} \times \mathbf{n}\right). \tag{10}$$

Thus, in a confined equilibrium, $\mathbf{M}$ will not generally be conserved, even though $\varepsilon_{\mathbf{l}} = 0$, because in general, neither the normal force λ vanishes, nor are $\mathbf{Y}$ and $\mathbf{n}$ parallel.

Let us now consider a curve confined by a surface with axial symmetry (about the the Z axis, say). The axisymmetric surface is described by the radial and height coordinates R and Z of the generators, parameterized by the arclength ℓ.[3] The azimuthal angle will be denoted by φ (see Appendix A). The curve is described by the embedding $s \to (\ell(s), \varphi(s))$, or $\Gamma : s \to \mathbf{Y}(s) = R(s)\hat{\boldsymbol{\rho}}(s) + Z(s)\hat{\mathbf{z}}$, where $\hat{\boldsymbol{\rho}}(s) = (\cos\varphi(s), \sin\varphi(s), 0)$. The tangent and conormal vectors are given by

$$\mathbf{T} = \cos\alpha\,\hat{\boldsymbol{\varphi}} + \sin\alpha\,\mathbf{e}_\ell\,, \qquad \mathbf{l} = -\sin\alpha\,\hat{\boldsymbol{\varphi}} + \cos\alpha\,\mathbf{e}_\ell\,, \tag{11}$$

where $\hat{\boldsymbol{\varphi}}(s) = (-\sin\varphi(s), \cos\varphi(s), 0)$ and $\mathbf{e}_\ell(s) = \dot{R}(s)\,\hat{\boldsymbol{\rho}}(s) + \dot{Z}(s)\,\hat{\mathbf{z}}$; α is the angle that the tangent of the curve makes with the azimuthal direction $\hat{\boldsymbol{\varphi}}$. Comparison with the expression (A2) for the embedding functions of an axisymmetric surface gives

$$\sin\alpha = \ell' \qquad \cos\alpha = R\,\varphi'\,. \tag{12}$$

Using Eqs. (11) and (12), the acceleration $\mathbf{T}'$ along the curve is given by

$$\mathbf{T}' = (\alpha' - \frac{R'}{R}\cot\alpha)\,\mathbf{l} - (\sin^2\alpha\,\kappa_\perp + \cos^2\alpha\,\kappa_\parallel)\,\mathbf{n}\,, \tag{13}$$

where $\kappa_\perp$ and $\kappa_\parallel$ are the principal curvatures along the meridians (generators with constant φ) and the parallels (circles of constant ℓ), respectively (see A). Thus the geodesic curvature of Γ, $\kappa_g = \mathbf{T}' \cdot \mathbf{l}$, is given by

$$\kappa_g = -\frac{(R\,\cos\alpha)'}{R\,\sin\alpha}\,; \tag{14}$$

the corresponding normal curvature $\kappa_n = -\mathbf{T}' \cdot \mathbf{n}$ is given by Euler's equation for the axisymmetric surface,

$$\kappa_n = \sin^2\alpha\,\kappa_\perp + \cos^2\alpha\,\kappa_\parallel\,. \tag{15}$$

Likewise the geodesic torsion τ_g is given by

$$\tau_g = \sin\alpha\cos\alpha(\kappa_\parallel - \kappa_\perp)\,. \tag{16}$$

Using the above expressions for the Darboux frame of a curve on an axisymmetric surface, along with the expression $\dot{Z} = R\,\kappa_\parallel$ (see Appendix A) and the identity $\cos\alpha\,\kappa_\parallel = -\cos\alpha\,\kappa_n - \sin\alpha\,\tau_g$, obtained by a linear combination of Eqs. (15) and (16), one finds that the torque about the symmetry axis, $M^Z = \mathbf{M} \cdot \hat{\mathbf{z}}$, is given by [26]

$$M^Z = R\left(-\sin\alpha\,(\kappa_g' + 2\,\kappa_n\,\tau_g) + \cos\alpha\left(\frac{\kappa_g^2 - \kappa_n^2}{2} - C\right)\right) + \dot{R}\,\kappa_g\,. \tag{17}$$

It is easy to confirm that this component is conserved: projecting Eq. (10) onto $\hat{\mathbf{z}}$, one gets

$$M^{Z\,'} = \mathbf{M}' \cdot \hat{\mathbf{z}} = \mathbf{Y} \cdot (\varepsilon_1\mathbf{l} \times \hat{\mathbf{z}} - \lambda\mathbf{n} \times \hat{\mathbf{z}})\,. \tag{18}$$

In an axisymmetric surface the three vectors $\mathbf{Y}$, $\mathbf{n}$ and $\hat{\mathbf{z}}$ are coplanar and $\mathbf{l} \times \hat{\mathbf{z}} = -\sin\alpha\hat{\boldsymbol{\rho}} - \cot\alpha R'\hat{\boldsymbol{\varphi}}$, therefore $M^{Z\,'} = -\sin\alpha\,R\,\varepsilon_1$, so it vanishes in equilibrium as claimed. Eq. (17) provides a first integral of the EL equation (7), which is not obvious by inspection.

To reconstruct the curve, the second order differential equation (17) needs to be solved for the angle α with fixed M^Z and C, and appropriate boundary conditions (BCs), which could be specifying the initial angle and its derivative (Cauchy BCs) or the angle at the boundaries (Dirichlet BCs). Once α is known, the position on the surface is determined using the relations (12). The two constants M^Z and C can be tuned to fix the length of the curve, L, and total azimuthal angle turned, $\Delta\varphi$.

III. CYLINDRICAL CONFINEMENT

Now we apply this framework to treat curves lying on a cylinder. Despite the apparent simplicity of the cylindrical geometry, the determination of the equilibrium configurations of curves on a cylinder is not straightforward. However, as explained below, the additional translational symmetry facilitates the integration of the EL equation.

———

[3] Derivatives with respect to ℓ will be denoted by an overdot, $\dot{} = \partial_\ell$.

A. Derivation of the quadrature

The height function is given by the meridian arc length, $Z = \ell$. We normalize all lengths in terms of the cylinder radius R_0. Scaled quantities will be denoted by lowercase letters or by an overbar, e.g. the scaled height function is $z := Z/R_0$. Curves on the cylinder will be parameterized by scaled arc length s/R_0.[4]

The scaled geodesic curvature is given by

$$\bar{\kappa}_g := R_0\, \kappa_g = \alpha' \,, \tag{19}$$

The two scaled principal curvatures are $\bar{\kappa}_\perp := R_0\, \kappa_\perp = 0$ and $\bar{\kappa}_\parallel := R_0\, \kappa_\parallel = 1$, so that the scaled normal curvature and geodesic torsion are given by

$$\bar{\kappa}_n := R_0\, \kappa_n = \cos^2 \alpha \,; \quad \bar{\tau}_g := R_0\, \tau_g = \sin\alpha \cos\alpha \,. \tag{20}$$

Inserting these expressions into the Euler-Lagrange equation (7), it is easily seen to read $(c = R_0^2\, C)$

$$\varepsilon_1 = \alpha''' + \alpha' \left(\frac{\alpha'^2}{2} + \frac{3}{2} \cos^4 \alpha - 6\, \sin^2 \alpha \cos^2 \alpha - c \right) = 0 \,. \tag{21}$$

The scaled first integral, Eq. (17), $(\mathbf{m} := R_0\, \mathbf{M})$ reads

$$m := \mathbf{m} \cdot \hat{\mathbf{z}} = -\sin\alpha \left(\bar{\kappa}_g' + 2\bar{\kappa}_n\, \bar{\tau}_g \right) + \cos\alpha \left(\frac{\bar{\kappa}_g^2 - \bar{\kappa}_n^2}{2} - c \right) \,. \tag{22}$$

On could now solve this third order differential equation (second order for α) following the procedure outlined at the end of the previous section. However it is possible to do better. We have yet to exploit the translational invariance along the cylindrical axis. When we do, we obtain a quadrature for α.

Translational invariance along $\hat{\mathbf{z}}$ implies that the projection of the scaled stress vector $\mathbf{f} := R_0^2 \mathbf{F}$ along the cylinder axis is constant. Projecting $\mathbf{f}$ onto $\hat{\mathbf{z}}$, and making use of definitions of $\mathbf{T}$ and $\mathbf{l}$ given in Eq. (11) one identifies the first integral

$$f := \mathbf{f} \cdot \hat{\mathbf{z}} = \cos\alpha \left(\bar{\kappa}_g' + 2\bar{\kappa}_n\bar{\tau}_g \right) + \sin\alpha \left(\frac{\bar{\kappa}_g^2 - \bar{\kappa}_n^2}{2} - c \right) \,. \tag{23}$$

It is straightforward to confirm that $f' = R_0^2\, \cos\alpha\, \varepsilon_1$.

Both first integrals are of second order in derivatives of α (this dependence enters through $\bar{\kappa}_g'$ in Eqs. (22) and (23)). One can now take an appropriate linear combination to eliminate this second derivative: specifically, the definition

$$\mu(\alpha) := m \cos\alpha + f \sin\alpha = \frac{\bar{\kappa}_g^2 - \bar{\kappa}_n^2}{2} - c \,, \tag{24}$$

will lead to a quadrature for α. Substituting for κ_g and κ_n one gets:

$$\frac{1}{2}(\alpha')^2 + U(\alpha) = c \,, \quad \text{where} \quad U(\alpha) = -\frac{\cos^4 \alpha}{2} - \mu(\alpha) \,. \tag{25}$$

It is not obvious at the level of the Euler-Lagrange equation that two integrations are possible. However, it should be remarked that the poor man's derivation of the quadrature using a variational principle adapted to symmetry demystifies this "coincidence". It is provided in Appendix B, a special instance of a more general construction presented in [26].

---

[4] Since there is no possible confusion, the scaled arc-length will also be denoted by s

One may ask if any additional information is to be gleaned by taking some other linear combination of f and m. Consider

$$\nu(\alpha) := -m \sin\alpha + f \cos\alpha = \bar{\kappa}'_g + 2\,\bar{\kappa}_n\,\bar{\tau}_g\,. \tag{26}$$

In terms of α this second order DE reads

$$\alpha'' + 2\cos^3\alpha\sin\alpha - \nu(\alpha) = 0\,. \tag{27}$$

On the one hand, taking into account expression (19), one has $\mu' = \nu\kappa_g$. On the other hand, using the identity for the cylinder $\bar{\kappa}'_n = -2\bar{\kappa}_g\,\bar{\tau}_g$, the derivative of the rhs of eq. (24) can be written as

$$\left(\frac{\bar{\kappa}^2_g - \bar{\kappa}^2_n}{2} - c\right)' = (\bar{\kappa}'_g + 2\,\bar{\kappa}_n\,\bar{\tau}_g)\kappa_g\,. \tag{28}$$

These two relations confirm that Eq. (26) follows from differentiation of Eq. (24). Alternatively, substituting identity (28) in Eqs. (22) and (23)) for m and f, and integrating them one obtains the quadrature (24). Further differentiation of Eq. (26) and substitution of the EL equation to replace κ''_g in favor of terms quadratic in the Darboux curvatures only reproduces Eq. (24).

The quadrature (25) provides us with an analogue of a particle with unit mass and energy c in a potential $U(\alpha)$. While the hard work lies ahead, this will prove to be very useful throughout this paper. That c plays the role of the energy in this identification is particularly appropriate, because c is also the conserved quantity, i.e. the Hamiltonian function, associated with the absence of an explicit dependence on s in the bending energy density, as detailed in Appendix B.

The first term in U, proportional to $\cos^4\alpha$ (or $\bar{\kappa}^2_n$), reflects the anisotropy of the sectional curvatures on the cylinder, which breaks the rotational symmetry about the normal vector. As a result, despite the fact that the cylinder is isometric to a plane, its extrinsic geometry is anisotropic and elastic curves on a cylinder behave differently from their counterparts on the plane. It is precisely this term that distinguishes elastic curves on the cylinder from their planar Euler elastic counterparts, which are integrable in terms of elliptic functions, as described in Appendix C. This can be see by introducing the change of variables $\alpha \to \psi + \beta$, $f \to F\sin\beta$ and $m \to F\cos\beta$. Now one has $\mu \to F\cos\psi$ and $\nu \to -F\sin\psi$, so without the κ^2_n term and its derivative, the quadrature (25) and the first integral (26) reduce to Eqs. (C8). If the curve lies close to a parallel or the cylinder has a very large radius, $R_0 \gg 1$, so that $\kappa_n \to 0$, $\tau_g \to 0$ and κ_g becomes the FS curvature of the curve on the plane, the two descriptions coincide. The comparison between the two will be discussed in Sec. IV B.

The two coordinate functions of the curve on the cylinder, are determined by the relations (12), which in terms of the scaled quantities reduce to

$$z' = \sin\alpha\,, \quad \varphi' = \cos\alpha\,. \tag{29}$$

B. Total bending energy and constraining force

The scaled bending energy of the constrained curve is given in terms of the angle α by

$$h_B := R_0\,H_B = \frac{1}{2}\int \mathrm{d}s\,(\alpha'^2 + \cos^4\alpha)\,. \tag{30}$$

Using the quadrature (24), the derivative can be eliminated in favor of α, so that

$$h_B = \int \mathrm{d}s\,\left(\cos^4\alpha + f\sin\alpha + m\cos\alpha + c\right)\,. \tag{31}$$

Taking into account the relations $z' = \sin\alpha$ and $\varphi' = \cos\alpha$, the last terms can be integrated

$$h_B = \int \mathrm{d}s\,\cos^4\alpha + f\Delta z + m\Delta\varphi + c\,l\,, \tag{32}$$

where $\Delta z = \Delta Z/R_0$, $\Delta \varphi$ and $l = L/R_0$ are the total scaled height, winding and scaled length of the curve. For a closed curve $\Delta z = 0$ and $\Delta \varphi = 2\pi p$. This relation makes explicit the respective interpretations of f, m, and c as coupling to the height, rotational extent and length.

Likewise, using the quadrature (25) and Eq. (27) to eliminate derivatives of α in the expression (8) for the magnitude of the scaled local constraining force on the cylinder, $\bar{\lambda} = R_0^3 \lambda$, can be expressed as

$$\bar{\lambda} \;=\; 2\,\bar{\kappa}_n^2\,(5 - 6\,\bar{\kappa}_n) + (6 - 11\,\bar{\kappa}_n)\,\mu - 4\,\bar{\tau}_g^2\,\nu + 6\,c\,(1 - 2\,\bar{\kappa}_n)\,, \tag{33}$$

or in terms of α and constants m, f and c

$$\bar{\lambda} = 2\,\cos^4\alpha\,(5 - 6\cos^2\alpha) - 6\,c\,\cos 2\alpha - 3\,f\,\sin\alpha\,(5\cos^2\alpha - 2) - 5\,m\,\cos\alpha\,(3\cos^2\alpha - 2)\,. \tag{34}$$

It depends only on the local value of the turning angle.

IV.   CLOSED EQUILIBRIUM CONFIGURATIONS

Now we will focus on isolated loops, i.e. closed curves without external sources of tension other than those due to confinement.[5] Let the loop have length $L = 2\pi R$, p be the number of times it winds the cylinder and n the number of periods in completing a circuit of the loop. Loops are characterized by p and n: loops with different p are homotopically inequivalent; n distinguishes equilibrium states within a given homotopy class. We will denote the sequence of loops with fixed values of these two integers, generated by varying the length of the loop by $\mathrm{L}_{p,n}$. Define the scaled total length $l = L/R_0 = 2\pi r$, where $r = R/R_0$ is the scaled radius of the loop. Since $l \geq 2\pi p$, the scaled radius is bounded from below by the number of windings, $r \geq p$. The length will be expressed in terms of the scaled excess radius $\Delta r = r - p \geq 0$.

We will examine loops that oscillate symmetrically about a parallel, which we set at $z = 0$ and refer to as the *equator*. This implies that the odd term linear in $\sin\alpha$ vanishes, so $f = 0$. Note that the potential U appearing in (25) now possesses up-down symmetry, $\alpha \to -\alpha$. However, the constant m does not necessarily vanish which breaks the left-right symmetry $\alpha \to \pi - \alpha$.

The tangent angle α will be bounded in a closed loop. It will now oscillate symmetrically between the turning points of the even potential, $-\alpha_M$ and α_M. These turning points will occur at the intersection of the loop with the equator; $\alpha = 0$ occurs on the two extremal parallels.

The two parameters m and c are determined by imposing the periodicity on the coordinates, required by the closure constraint. Note, first of all, that closure in the axial direction is consistent with $f = 0$. To see this, note that for a closed curve, after one half period one has $\Delta z = 0$ [18, 20]; using the quadrature (25) and the relation (29 connecting z to α one has

$$\Delta z = \frac{1}{\sqrt{2}} \int_{-\alpha_M}^{\alpha_M} d\alpha\,\frac{\sin\alpha}{\sqrt{c - U(\alpha)}} = 0\,. \tag{35}$$

This is because $U(\alpha)$ is an even function of α so that the integrand is odd.

The remaining two parameters m and c can be related to the three geometric quantities p, n and Δr by integrating the quadrature (25) along with the relation connecting φ to α, (Eq. (29)) using the fact that the azimuthal range $\Delta\varphi$ is quantized: i.e. $\Delta\varphi/(2\pi) = p$. One obtains

$$\Delta r \;=\; \frac{4\,n}{\sqrt{2}\,2\,\pi} \int_0^{\alpha_M} d\alpha\,\frac{1}{\sqrt{c - U(\alpha)}} - p\,, \tag{36a}$$

$$p \;=\; \frac{4\,n}{\sqrt{2}\,2\,\pi} \int_0^{\alpha_M} d\alpha\,\frac{\cos\alpha}{\sqrt{c - U(\alpha)}}\,. \tag{36b}$$

----

[5] Recall that we ignore polymer twist, so one might wonder whether this could change the solutions. However, if the polymer is rotationally symmetric, having no "preferred side" for it to adhere onto the surface and no preferred bending direction, any local twist does not couple to the surface constraint, and so we only need to consider the *global* constraint. If we now start with an untwisted circle and imagine extending its length in such a way that no twist is added, ignoring twist right from the start is permissible.

In Eq. (36b) we have used the fact that α completes n periods while the loop completes p trips around the cylinder.

Before analyzing the loops in the nonlinear regime, we will first solve the quadrature in a perturbative manner for loops which deviate slightly from a circular loop covering the equator p times. The insight we obtain will prove to be useful when solving the quadrature (25) numerically.

A. Perturbative solutions about a circular loop

To examine deformations of a circular loop perturbatively, we let α_1 represent a small perturbation about $\alpha_0 = 0$. We set $f = 0$ and expand the constants, $m = m_0 + m_2 + \ldots$ and $c = c_0 + c_2 + \ldots$,[6] . The subindices represent the order in the expansion. The approximation of the quadrature (25) at lowest order reads

$$m_0 = -c_0 - \frac{1}{2} \, ; \tag{37}$$

Note that m_0 and c_0 appear in the combination $m_0 + c_0$ which is constant independent of n and p. At second order the quadrature describes harmonic oscillations:

$$\frac{1}{2} \left(\alpha_1'\right)^2 + V_2(\alpha_1) = E_2 \, , \tag{38}$$

where we have defined

$$V_2(\alpha_1) = a_0 \, \alpha_1^2 \, , \quad a_0 = m_0/2 + 1 \quad \text{and} \quad E_2 = m_2 + c_2 \, . \tag{39}$$

Thus the behavior of the perturbation can be described in analogy to a particle of unit mass and energy E_2 moving in a quadratic potential V_2. The parameter a_0 is necessarily positive. Otherwise V_2 would be a downward parabola, α would not be periodic, and the corresponding loops would be open.

The two turning points of V_2, corresponding to the maximum and minimum values of α, are $\pm\alpha_{M1}$, where

$$\alpha_{M1} = \frac{\sqrt{2E_2}}{q} \quad \text{and} \quad q^2 := 2a_0 = m_0 + 2 \, . \tag{40}$$

Solving Eq. (38) one identifies

$$\alpha_1 = \alpha_{M1} \, \cos q \, s \, ; \tag{41}$$

combining Eqs. (37) and (40), m_0 and c_0 can be expressed in terms of q

$$m_0 = q^2 - 2 \, , \quad c_0 = \frac{3}{2} - q^2 \, . \tag{42}$$

The condition that the periodic perturbation should complete n periods, while the curve winds p times around the cylinder implies that the wave number is given by the ratio of periods to windings,

$$q = \frac{n}{p} \, . \tag{43}$$

Notice that m_0 does not vanish because q is a rational number. A critical axial torque is required to deform a loop of radius R_0 into a state with a given ratio q. In particular, m_0 is negative when $n = 1$ and positive for all higher values of n. This sign change has physical significance. Superficially, states with the same p and different values of n may appear to be identical when $\Delta r = 0$. However, as we will see, the different values of m_0 and c_0 in these states determine the critical buckling forces required to initiate the deformation of the circular loop into the appropriate state.

———

[6] First order terms will not be considered, because they will be proportional to first order changes in the length of the circle, which vanishes on account of the geodesic character of the parallel.

From the relation (40) between E_2 and α_{M1}, one concludes that the sum of their second order corrections is constrained by the amplitude

$$E_2 = m_2 + c_2 = \frac{q^2}{2}\, \alpha_{M1}^2\,. \tag{44}$$

To identify a second relation between m_2 and c_2 we use the conditions (36), which relate the excess radius and the azimuthal range in terms of the potential. Since to first order the turning points are $\pm \alpha_{M1}$, the denominator in these expressions can be expanded as

$$c - U(\alpha) \approx (\alpha_{M1}^2 - \alpha_1^2)(\chi - \xi \alpha_1^2)\,, \tag{45}$$

where

$$\chi = \frac{1}{2}\,(q^2 + m_2) - \xi \alpha_{M1}^2\,, \quad \xi = \frac{1}{24}\,(18 + q^2)\,; \tag{46}$$

thus

$$\frac{1}{\sqrt{2}\,\sqrt{c - U(\alpha)}} \approx \frac{1}{q\sqrt{\alpha_{M1}^2 - \alpha_1^2}} \left[1 + \frac{1}{q^2}\left(\xi\,(\alpha_{M1}^2 + \alpha_1^2) - \frac{m_2}{2}\right)\right]\,. \tag{47}$$

Substituting this expression into the two conditions (36) and integrating, one obtains

$$\Delta r = \frac{p}{2\,q^2}\,(3\,\xi\,\alpha_{M1}^2 - m_2)\,, \quad m_2 = \left(3\,\xi - \frac{q^2}{2}\right)\alpha_{M1}^2\,. \tag{48}$$

From these two equations one finds that the excess radius is proportional to the square of the perturbation amplitude

$$\Delta r = \frac{p}{4}\,\alpha_{M1}^2\,. \tag{49}$$

Using this relation in Eqs. (44) and (48) one can express m_2 and c_2 in terms of the excess radius:

$$m_2 = \frac{3}{p}\left(3 - \frac{1}{2}\,q^2\right)\Delta r\,, \quad c_2 = \frac{1}{p}\left(\frac{7}{2}\,q^2 - 9\right)\Delta r\,. \tag{50}$$

To complete the construction of the constrained curve one needs to determine its position coordinates z and φ by integrating the relations (29). To first order

$$z_1' = \alpha_1\,, \quad \varphi_1' = 0\,; \tag{51}$$

consequently This confirms to first order that a non-vanishing value of the conserved axial force f is inconsistent with closed deformations of a parallel circle. Note first that, if $f \neq 0$, the potential V_2 defined in Eq. (39) gains up a linear term so that z_1 picks up a helical contribution proportional to arclength, which is inconsistent with closure.

$$z_1 = \frac{2}{n}\,\sqrt{p\,\Delta r}\,\sin qs\,, \quad \varphi_1 = 0\,. \tag{52}$$

In contrast to its spherically confined counterpart, the elliptic deformation of an elastic loop on a cylinder with $n = 1$ and $p = 1$ is not identified with a rotation, but with a tilt of the loop extending its length.

1. Energy and confining force of perturbed loops

In the quadratic approximation the bending energy h_B is given by

$$h_B \approx \pi\,\left(p + \left(2\,q^2 - 3\right)\Delta r\right)\,. \tag{53}$$

Using the fact that $r^{-1} \approx p - \Delta r$, the energy can also be expressed in terms of the energy of the circle with reduced radius r, $h_c = \pi/r$ as

$$h_B \approx h_c\,\left[1 + 2\,\left(q^2 - 1\right)\Delta r\right]\,. \tag{54}$$

It is now manifest that at lowest order the energy of the deformed loop is given by the energy of the circular loop, $h_B \approx h_c$. The second order correction to the energy of the loop vanishes for elliptic perturbations with $q = 1$, whereas it increases (decreases) if $q > 1$ ($q < 1$).

To second order, the magnitude of the normal force $\bar{\lambda}$ given by Eq. (34) reads

$$\bar{\lambda} \approx q^2 - 1 + \frac{1}{p} \left[q^2 \left(11 \cos 2q\varphi - \frac{5}{2} \right) + 7 - 2 \cos 2q\varphi \right] \Delta r \,. \tag{55}$$

For the elliptical confined states with $q = 1$, only the second order correction is non-zero, $\bar{\lambda} \approx 18 \left(\cos^2 \varphi - \frac{1}{4} \right) \Delta r$. It vanishes in the limit $\Delta r \to 0$. Note that $\bar{\lambda}$ is not positive everywhere, assuming negative values in the two intervals $\varphi \in (\pi/3, 2/3\pi)$ and $\varphi \in (-2/3\pi, -\pi/3)$, describing the neighborhood of the turning points where the height is a maximum and a minimum. On account of this, if the loop is bound inside the cylinder and free to detach, one expects that it will tend to rotate into the vertical plane, touching the cylinder tangentially at two points. Such states are described exactly by two segments of a planar Euler elastic curve as described in Appendix C. A loop bound to the outer side of the cylinder, free to detach, will tend to detach on the equator first before reforming as a circular loop.

Note that a constant normal force $\bar{\lambda}_0 = q^2 - 1$ persists in the limit $\Delta r \to 0$ in all other states. This behavior is analogous to the Euler instability associated with n-folds confined by a sphere [27].[7] In general, $\bar{\lambda}_0$ is positive (negative) if $q > 1$ ($q < 1$), so initially the loop will push (constrict) everywhere on the cylinder. In particular, an interior bound curve with $p = 1$ and n-fold dihedral symmetry will push on the cylinder whereas its exterior counterpart will peel off.

Whereas the second order correction to the transmitted force can have either sign (correlating with the sign of the cosine of the double angle) one has to proceed beyond perturbation theory to determine if the sign of the force in non-elliptical states changes in longer loops, as we will see in Sec. IV B, it does).

An interior bound figure of eight ($n = 1$, $p = 2$) would be expected to unwind into the planar Euler elastic vertical confined state; an exterior one, on the other hand will constrict the cylinder. Note that this configuration possesses a lower energy than a free twice-covered circular loop. There is no inclination to detach from the cylinder. With increased length, as we will see in our non-perturbative treatment of the problem, we would not expect this state to remain completely attached; intuitively we would nonetheless expect it to continue to constrict the cylinder. The topological obstruction provided by the cylinder prevents the doubly wound elastic loop from unraveling into its singly wound ground state. This will be confirmed when we venture beyond perturbation theory. An exterior bound loop wound more than once around a cylinder will always constrict the cylinder.

2. Stability of perturbed loops

Modulo the EL equation, the second variation of the energy is given by

$$\delta^2 H_B = \int \mathrm{d}s \, \Phi \mathcal{L} \Phi \,, \tag{56}$$

where $\mathcal{L}$ is a self-adjoint fourth order differential operator, defined at lowest order and about a p-fold covering of the equator by

$$\mathcal{L} = \frac{\partial^2}{\partial s^2} \left(\frac{\partial^2}{\partial s^2} + q^2 \right) \,, \tag{57}$$

and Φ is the normal deformation along $\mathbf{l}$, $\Phi = \delta \mathbf{Y} \cdot \mathbf{l}$. On account of the fixed length condition, the permissible normal deformations ought to be orthogonal to the geodesic curvature, so Φ must satisfy the global constraint [42]

$$\oint \mathrm{d}s \, \kappa_g \, \Phi = 0 \,. \tag{58}$$

---

[7] Its relation to the non-vanishing axial torque (m_0) associated with the confined loop in this limit is somewhat mysterious.

The eigenmodes of $\mathcal{L}$ are $1, \varphi, \cos Q\varphi, \sin Q\varphi$.[8] Since the periodic eigenmodes ought to have the same number of windings as the original loop, the wave number is given by $Q = k/p$ where k is another integer. Their corresponding eigenvalues are

$$C_k = \frac{k^2}{p^4}\left(k^2 - n^2\right). \tag{59}$$

There are four zero modes with $C_k = 0$, the constant and linear modes 1 and φ and two (cosine and sine) eigenmodes with the same number periods as the original loop, $k = n$ $(Q = q)$. However, the eigenmode φ is not periodic and the eigenmode $\cos q\varphi \propto \kappa_g$ does not satisfy the global isometry condition (58), so both of these modes will not be considered. The allowed zero modes correspond to a translation along $(\Phi_T = 1)$ and a rotation about $(\Phi_R = \sin q\varphi \propto \kappa_g')$ the axis of the cylinder.

In Fig. 2 the eigenvalues C_k are plotted for the first n-fold perturbations of a single covering of the equator $(q = 1)$. These eigenvalues are all positive for the elliptic state with $n = 1$. All states with $n \geq 2$, however, exhibit negative eigenvalues, which signal the possibility of decay to states with lower energy, if they are accessible. Therefore, in this approximation only the elliptical state $n = 1$ is stable, whereas the higher n-folds with $n \geq 2$ are unstable. Of course, to access the stability of the elliptic ground state one need to also treat perturbations lifting the loop off the surface. In the absence of an adhesive force one would expect this state to be unstable with respect to such perturbations.
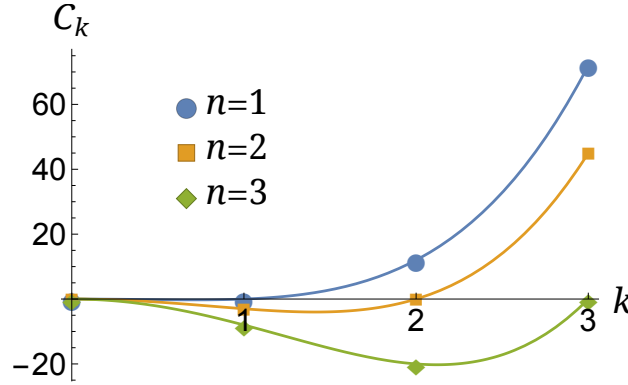

FIG. 2: Eigenvalues C_k corresponding to deformations of a parallel circle. For all $n > 1$, the spectrum posesses a negative eigenvalue.

B. Non-linear regime

We now examine loops in their full non-linear glory. Their analysis is again facilitated by exploiting the analogy with a particle in a periodic potential.

First, the constant c can be cast in terms of the turning points of U and m: let $\alpha' = 0$ at $\alpha = \pm\alpha_M$ in the quadrature Eq. (25) then

$$c = -\frac{1}{2}\cos^4\alpha_M - m\cos\alpha_M. \tag{60}$$

For a circular loop this reproduces Equation (37), relating c and m to lowest order in perturbations. c vanishes if the curve is vertical on the equator $(\alpha_M = \pi/2)$ or when $m = -1/2\cos^3\alpha_M$ $(\alpha_M \neq \pi/2)$. The relationship (60) permits us to recast the quadrature in terms of α_M and m: $\alpha'^2 = V(\alpha)^2$, where

$$V(\alpha)^2 \equiv 2\left(c - U(\alpha)\right) = \left(\cos\alpha - \cos\alpha_M\right)\left[\left(\cos\alpha + \cos\alpha_M\right)\left(\cos^2\alpha + \cos^2\alpha_M\right) + 2m\right]. \tag{61}$$

---

[8] Recall that to lowest order s is given by φ.

Since $\pi \geq \alpha_M \geq \alpha \geq 0$, one has $\cos \alpha \geq \cos \alpha_M \geq 0$, so $V^2 \geq 0$ implies the lower bound on the axial torque, $m \geq -2 \cos^3 \alpha_M$; thus there are no closed curves with $m < -2$. Eq. (60) now implies the bounds on c, $c \leq 3/2 \cos^4 \alpha_M$ for $0 < \alpha_M < \pi/2$ ($c > 3/2 \cos^4 \alpha_M$ for $\pi/2 < \alpha_M < \pi$). These bounds together imply the inequality $c \leq 3/2(|m|/2)^{4/3}$.

For a given p-fold covering and n-fold dihedral symmetry, Eq. (36b) establishes the relationship between m and α_M. Curiously, this is independent of the length of the loop. Modulo this condition, α_M or m is determined as a function of Δr using Eq. (36a). To trace the trajectory of the loop one integrates the quadrature for a given Δr to obtain α as a function of ℓ; the relations (29) permit one to position the loop on the cylinder.

The functional relationship between m and α_M is presented in Fig. 3 for each of the three sequences, $L_{2,1}$ (blue curve), $L_{1,1}$ (black) and $L_{1,2}$ (red). While this may be the first relationship to be established, the information it conveys is not immediately transparent.[9] It is somewhat easier to understand the behavior of m and α_M as functions of Δr. In Fig. 4(a), 4(b) and 4(c) α_M, m and c are plotted as functions of loop length for each of the three sequences. We see that m increases towards a maximum in each sequence. The corresponding loops with maximum values of m are illustrated in Figs. 5(c), 6(b) and 7(d), respectively. Beyond this single maximum m decreases monotonically to zero. The axial torque vanishes in all long loops. In each of the $L_{2,1}$ and $L_{1,1}$ sequences, m changes sign from negative to positive at some finite Δr. In particular, there is a finite value of Δr at which the axial torque vanishes. This does not, of course, mean that the total torque vanishes.[10] These states are tractable analytically and will be discussed in detail in Appendix D. Surprisingly, one finds that α_M does not increase monotonically with loop length. It increases from its value $\alpha_M = 0$ reaching a maximum value ($> \pi/2$) before returning asymptotically to $\pi/2$ in long loops. At some critical length on the way up, $\alpha_M = \pi/2$, indicating that the loop develops vertical tangents on the equator. In these states the constant c vanishes, which indicates that they are also special with respect to length. Loops with values of $\alpha_M > \pi/2$ develop overhangs on each side of the equator.
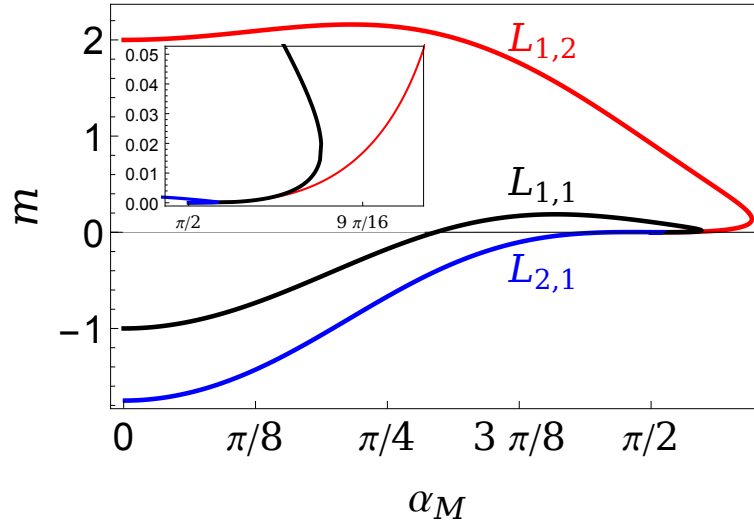

FIG. 3: (Color online) Behavior of the vertical torque m as a function of α_M for the sequences $L_{2,1}$ (blue curve), $L_{1,1}$ (black curve) and $L_{1,2}$ (red curve). The complicated relationship between m and α_M upon the development of vertical tangents with $\alpha_M \pi/2$ (detailed in the inset) is clarified by examining separately the functional dependencies of m and α_M on Δr.

---

[9] Note, however, that it is consistent with the perturbative behavior presented in Sect. IV A for small α_M. Recall that for a p-fold covering of the equator, with $\alpha = \alpha_M = 0$, one has $m = (n/p)^2 - 2$. (See Eqs. (42).) The leading correction is quadratic in α_M, $m_2 = \frac{3}{4} \left(3 - \frac{1}{2} (n/p)^2\right) \alpha_M^2$.

[10] Likewise $\mathbf{M}$ does not vanish in long loops. For while they are stretched along the cylinder, as we will see, the asymptotic geometry is non trivial.
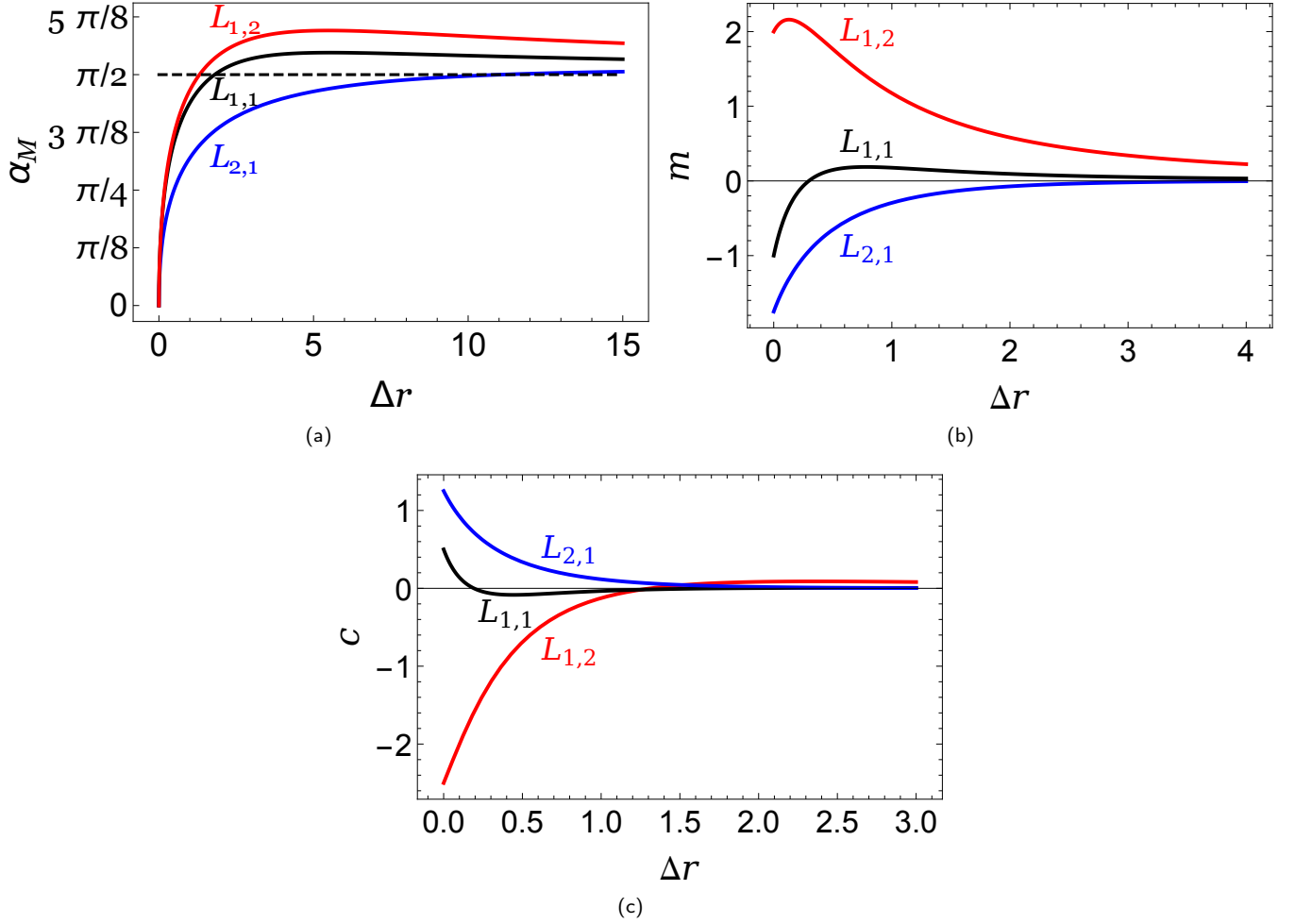
FIG. 4: (Color online) (a) Behavior of (a) α_M and (b) Axial torque m and (c) Parameter c as function of excess radius Δr for each of $L_{2,1}$ (blue curve), $L_{1,1}$ (black curve) and $L_{1,2}$ (red curve) sequences. In all three cases α_M initially increases with Δr from a value $\alpha_M = 0$ when $\Delta r = 0$. The corresponding states are loops covering the equator described by perturbation theory. α_M reaches a maximum ($> \pi/2$) at a finite value of Δr. There is a critical intermediate loop length at which $\alpha_M = \pi/2$ where the loop develops vertical tangents. As the length is increased α_M falls asymptotically to $\pi/2$ corresponding to a loop stretched along the cylinder. The axial torque initially increases with Δr ($m = (n/p)^2 - 2$ when $\Delta r = 0$), reaching a maximum, tending to zero as Δr becomes large. $c_0 = 3/2 - (n/p)^2$ when $\Delta r = 0$ and $c \to 0$ when Δr is large. Its vanish correlates with $\alpha_m = \pi/2$.

1. $L_{1,1}$ ground state

Equilibrium loops completing one period in one trip around the equator are represented in Fig. 5 focusing on the behavior as the length of the loop is increased. If Δr is small, the loop is a tilted ellipse described accurately by perturbation theory about the equator. See Fig. 5(a). As the length increases, the eccentricity of this loop increases obliging it to tilt away from the equatorial plane (Fig. 5(b)); it also begins to bend out of the plane of the ellipse (Fig. 5(c)) as inflections develop at the equatorial crossings (Fig. 5(d)). This out of plane bending can be viewed as a consequence of the mismatch between the curvature within the two hairpins which follow the parallel circles on the cylinder and the increasing linearity of the sections interpolating between them. At some point the tangents on the equator become vertical with $\alpha_M = \pi/2$. With increased length, overhangs appear and the loop develops lobes on either side of the equator. With increased Δr, the lobes, however, continue to grow (Fig. 5(e)).[11] At some critical

---

[11] The angle α_M, on the other hand, reaches a maximum, returning asymptotically to $\pi/2$.

length the two lobes make self-contact at the back of the cylinder (Fig. 5(f)). Meanwhile the two section interpolating between the hairpins becomes increasingly vertical. The loop will eventually self-intersect. Very long loops consist of two hairpins connected by two very long self-intersecting almost vertical sections. Both the length of these sections and a number of self-intersections along them is approximately proportional to the length of the loop.
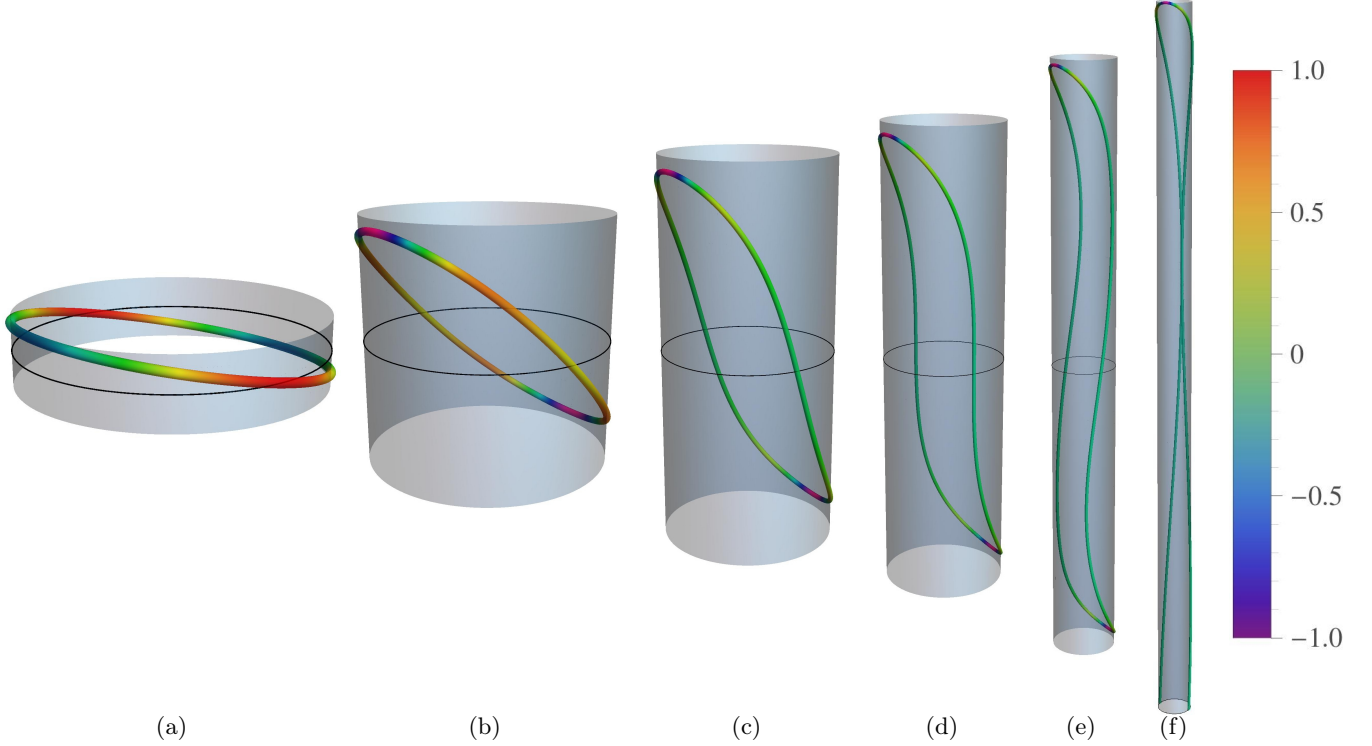

FIG. 5: (Color online) $L_{1,1}$ loop sequence. (a) $\Delta r = 0.01$ ($\alpha_M \approx \pi/16$), (b) $\Delta r = 0.192$ ($\alpha_M \approx \pi/4$ and $h_{B\,\mathrm{min}}$), (c) $\Delta r = 0.78$ ($\alpha_M \approx 2\pi/5$ and m_{max}), (d) $\Delta r = 1.8$ ($\alpha_M = \pi/2$ and $h_{B\,\mathrm{max}}$), (e) $\Delta r = 5.544$ ($\alpha_{M\,\mathrm{max}} \approx 0.548\,\pi$) and (f) $\Delta r = 27.819$ ($\alpha_M \approx 0.522\,\pi$, first self-contact occurs). In (f) only the upper half of the loop is displayed. The normalized magnitude of the normal force λ is color coded along the loop in these figures.

2. $L_{1,2}$ excited states

Significant features of loops undergoing two periods while they wrap the cylinder once are represented in Fig. 6. If the loop is short, it consists of a small oscillation about the equator, (Fig. 6(a)), the amplitude of the oscillation increasing with length (Fig. 6(b) and (c)). When $\Delta r = 1.313$ the loop becomes vertical at the equator, (Fig. 6(d)). Lobes develop in longer loops with α_M reaches its maximum when $\Delta r = 5.48$ (Fig. 6(e)). The first self-contact occurs when $\Delta r = 8.59$ (Fig. 6(f)). Self-intersections will occur in longer loops. Asymptotically, states consist of four hairpin bends interpolated by increasingly vertical mutually intersecting sections. One can also think of this state as a folded $n = 1$ state, with the folds themselves forming hairpins. In general, states with $n > p$ will behave in a manner similar to those in this sequence.

3. $L_{2,1}$ states

Non-trivial loops which wind about the cylinder more than once ($p > 1$) are also possible whenever $r \geq p$. The $L_{2,1}$ loop sequence is represented in Fig. 7. If the excess length is small the loop approximates a double covering of the equator, adopting as the length is increased the shape of a folded figure of eight wrapping the cylinder, with its self-intersection lying on the equator. See Fig. 7(a). (If $p = 3$, the two intersections migrate off the equator.) The crossing angle increases as the figure is stretched. See Figs. 7(b)-(d). This angle becomes vertical when $\Delta r = 11.06$, see Fig. 7(e). α_M reaches a maximum value $0.51\,\pi$, at $\Delta r = 27.548$. See Fig. 7(f). In longer loops, additional
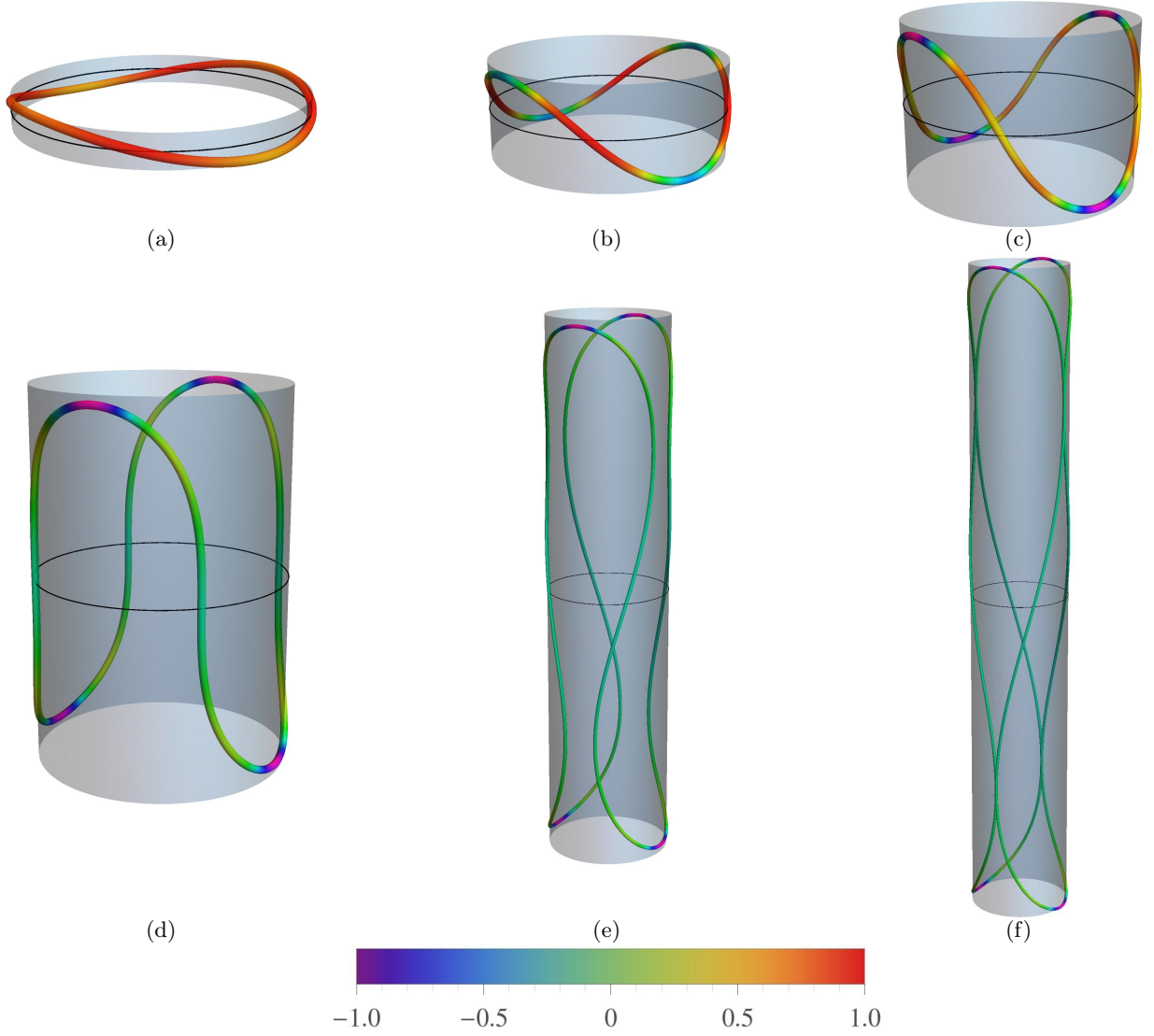
FIG. 6: (Color online) $L_{1,2}$ loops sequence. (a) $\Delta r = 0.01$ ($\alpha_M \approx \pi/16$), (b) $\Delta r = 0.13$ ($\alpha_M \approx 0.216\pi$ and $m_{\max}$), (c) $\Delta r = 0.365$ ($\alpha_M = \pi/3$), (d) $\Delta r = 1.313$ ($\alpha_M = \pi/2$ and $h_{B\max}$), (e) $\Delta r = 5.48$ ($\alpha_{M\max} \approx 0.595\,\pi$) and (f) $\Delta r = 8.59$ (first self-contact occurs, $\alpha_M \approx 0.588\,\pi$). The normalized magnitude of the normal force λ is color coded in these figures.

self-intersections appears above and below the equator. In contrast to the asymptotic behavior of the $L_{1,1}$ sequence, the two hairpins lie on the same meridian.

The appearance of the self-intersections in these three sequences of loops can be understood more easily by unfolding them as described in detail in Appendix E.

4. Trajectories in the c-m parameter space

For completeness, we also represent the three sequences as trajectories in the $c - m$ parameter space. These trajectories are bounded by two curves,

1. The line $m = -1/2 - c$, denoted by Π, representing loops covering the equator p times, is indicated by the gray dashed line in Fig. 8.

2. The curve $c = 3/2(|m|/2)^{4/3}$, denoted Υ representing loops saturating the inequality between c and m, is indicated by the gray dotted curve in Fig. 8.
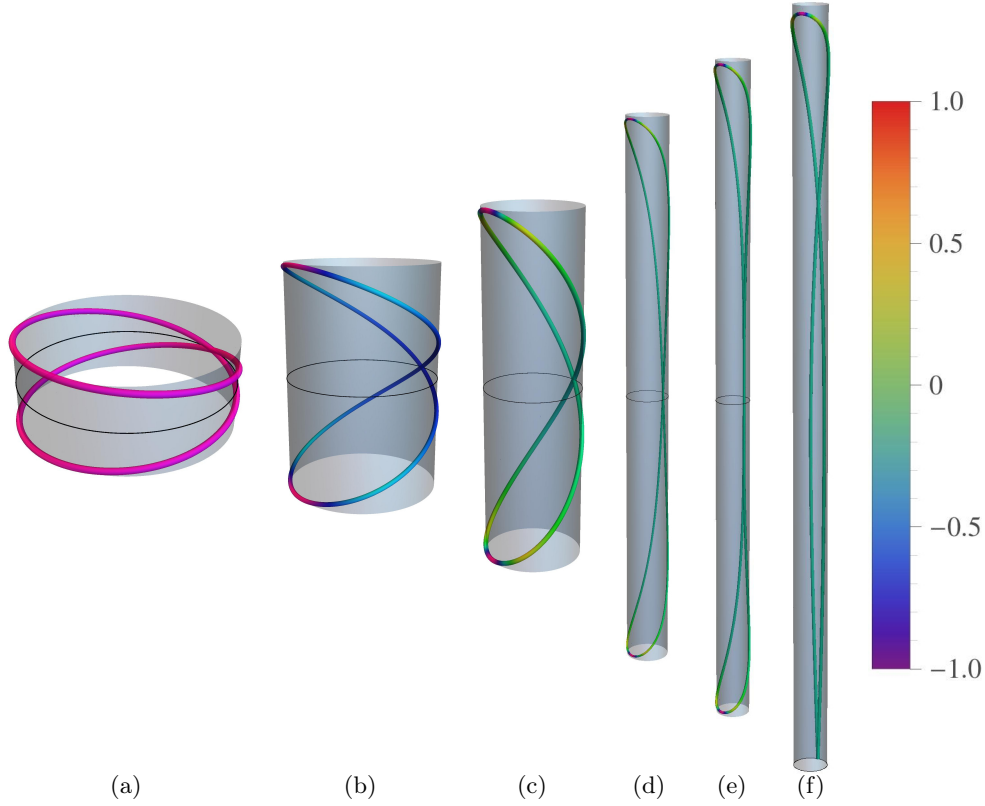
FIG. 7: (Color online) Loops of sequence $L_{2,1}$. (a) $\Delta r = 0.02$ ($\alpha_M \approx \pi/16$), (b) $\Delta r = 0.25$ ($\alpha_M \approx 0.194\,\pi$), (c) $\Delta r = 1.149$ ($\alpha_M = \pi/3$), (d) $\Delta r = 6.916$ ($\alpha_M \approx 0.48\pi$ and $m_{\max}$), (e) $\Delta r = 11.06$ ($\alpha_M = \pi/2$ and $h_{B\,\max}$) and (f) $\Delta r = 27.548$ ($\alpha_{M\,\max} \approx 0.51\,\pi$). In (f) only the upper half is displayed. The normalized magnitude of the normal force λ is color coded in these figures.

The point $(3/2, -2)$ at the intersection of Π and Υ, is a limit point, corresponding to loops winding the equator an ever increasing number of times ($p \to \infty$), with a finite number of periods, so that $c_0 \to 3/2$ and $m_0 \to -2$.

All three trajectories originate on Π and terminate at the origin. Infinitely long loops have vanishing m and c. In this limit the fixed length constraint gets relaxed as c becomes vanishingly small.

The trajectory for $L_{1,1}$ ($L_{2,1}$) indicated by the black (blue) curve in Fig. 8 begins at the point $(1/2, -1)$ $((5/4, -7/4))$ spiraling towards the origin. Both trajectories cross the line $c = 0$ three times; twice with a finite value of m, one with an acute angle and another with vertical tangents at the equator, and again at the origin.

Likewise the trajectory for $L_{1,2}$ begins on Π at $(-5/2, 2)$ but it forms an arc, crossing the line $c = 0$ twice, once where the loop has vertical tangents and again at the origin.

In general, any sequence with $n > p$ begins on Π to the left of $L_{1,1}$, whereas sequences with $n < p$ begin on the right, all sequences tend asymptotically to the origin. Sequences with $c > 0$ ($c < 0$) or $n/p < \sqrt{3/2}$ ($n/p > \sqrt{3/2}$) will cross the line $c = 0$ three times (twice) and thus will have spiral-like (arc-like) trajectories as in sequence $L_{2,1}$ ($L_{1,2}$).

5. Total energy

Loops in the $L_{p,n}$ sequence originate in p-fold coverings of the equator. Thus their initial energy is $h_B = \pi\,p$, independent of n. See Fig. 9. If the excess radius Δr is small, loop states in the $L_{1,1}$ sequence are approximately elliptic; their energy is thus close to that of their planar vertical counterparts presented in Appendix C, as revealed by the initial coincidence of the solid black and gray curves respectively in Fig. 9. However, in this sequence the energy
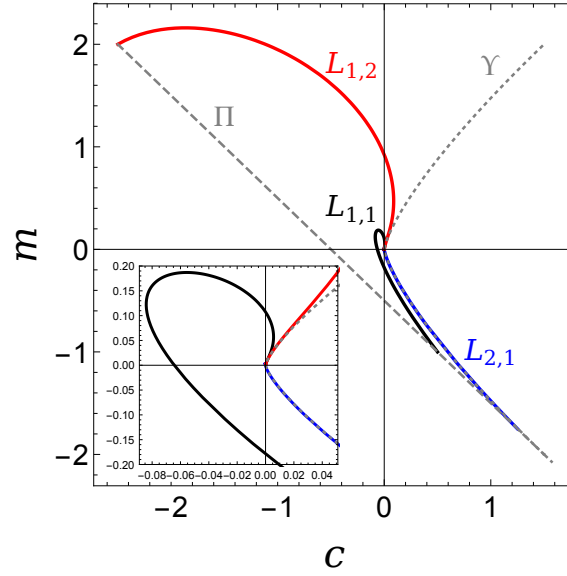
FIG. 8: (Color online) Trajectories in the parameter space $c - m$ of sequences $L_{2,1}$ (blue curve), $L_{1,1}$ (black curve) and $L_{1,2}$ (red curve). Dashed line Π represent the bound $m = -1/2 - c$, corresponding to a single or multiple covering of the equator, whereas dotted line Υ represent the bound $c = 3/2(|m|/2)^{4/3}$ and correspond to loops covering the equator a very large number of times. The intersection of Π and Υ occurs at the point $(3/2, -2)$. The inset shows the trajectories in the neighborhood of the origin, corresponding to loops with very large excess radius.

reaches a global minimum when $\Delta r = 0.192$, corresponding to the state illustrated in Fig. 5(b), increasing towards a global maximum value $h_B = 1.042\,\pi$ when $\Delta r = 1.80$ (the state with $\alpha_M = \pi/2$ and $c = 0$), after which it decreases asymptotically towards $h_B = \pi$. Long loops and short ones have the same energy! By contrast, the energy of planar vertical loops decreases monotonically to a minimum value of 0.914π when $\Delta r = 0.393$ which is when the curvature in the free loop vanishes where it makes contact with the wall. Thereafter it remains constant because any additional length gets directed into the straight line segments. See the inset in Fig. 9. We see that vertical loops always have lower energy than any bound counterpart: the former thus provides the ground state of interior bound loops allowed to unbind.

The energy of excited states in the $L_{1,2}$ sequence is indicated by the red line in Fig. 9. While it is initially degenerate with the $L_{1,1}$ sequence, with energy $h_B = \pi$, unlike the latter it increases with the excess radius from the beginning, reaching a maximum at $\Delta r = 1.313$ (also when $\alpha_M = \pi/2$), thereafter decreasing asymptotically to the value $h_B = 2\,\pi$. The energy of the double winded $L_{2,1}$ sequence is indicated by the blue curve in Fig. 9. It starts at $h_B = 2\,\pi$; unlike the energy of the $L_{1,1}$ sequence which only decreases initially, the energy decreases monotonically to $h_B = \pi$, the same asymptotic energy as a loop in the $L_{1,1}$ sequence.

In general, for $L_{p,n}$ sequences with $n > p$, the maximum of h_B occurs in states with vertical tangents on the equator and finite vertical torque, i.e. $\alpha_M = \pi/2$ and $m \neq 0$. The corresponding states in the $L_{1,1}$ and $L_{1,2}$ sequences are displayed in Figs. 5(d) and 7(e). For $n < p$ the initial states possess the maximum energy within the sequence. Since loops with very large excess radius are essentially straight almost everywhere, the principal contributions to the total energy will be from the $2\,n$ curved hairpins, each with approximately the same energy as a semicircle, $h_B = \pi/2$. This explains the coincidental simplicity of the asymptotic energy in the three sequences: for all $L_{p,n}$, the energy $h_B \to \pi\,n$ (from above) as $\Delta r \to \infty$. It is independent of the topology of the loop.

6. Transmitted normal force

The magnitude of the normal force $\bar{\lambda}$, scaled to lie between -1 and 1, is represented in color along the loops in Figs. 5, 6 and 7, indicating clearly the regions where they are pushing or pulling the cylinder: red (purple) represent
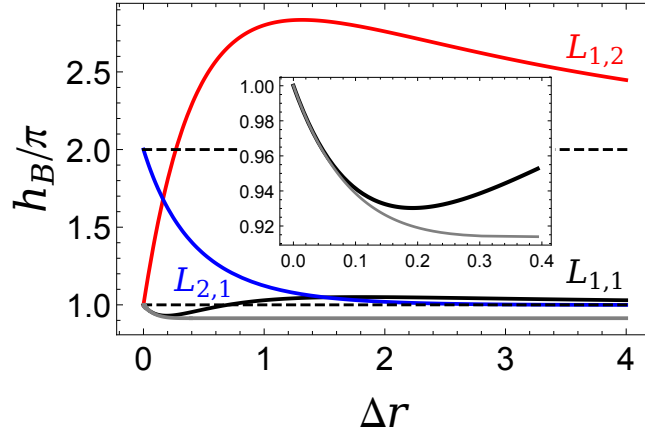
FIG. 9: (Color online) Total energy of loops belonging to the three sequences $L_{2,1}$ (blue), $L_{1,1}$ (black) and $L_{1,2}$ (red), as well as the energy of the vertical loop touching the cylinder along its sides (gray). The initial value of the total energy of the $L_{p,n}$ sequence is $h_B = \pi p$ corresponding to a p-fold covering of the equator, whereas the energy of loops with very large excess radius tend asymptotically to the value $h_B = \pi n$, indicated with dashed lines.

regions where the push (pull) is maximum,[12] whereas green represent regions in which the transmitted force is low. In general, it is observed that the maximum push occurs at the equatorial crossings, whereas the minimum (maximum pull if negative) occurs at the hairpins. The maximum (solid curves) and minimum (dashed curves) values of $\bar{\lambda}$ are plotted as function of the excess radius Δr in Fig. 10(a) for each of the three $L_{1,1}$ (black curve), $L_{1,2}$ (red curve) and $L_{2,1}$ (blue curve) sequences.

The perturbative result, Eq. 55, indicates that the initial state of a sequence $L_{p,n}$ exerts a normal force of magnitude

$$\bar{\lambda}_0 = (n/p)^2 - 1 \,. \tag{62}$$

Regardless of n and p, the maximum and minimum values of $\bar{\lambda}$ tend to $\bar{\lambda}_{max} \to 1$ approximately and $\bar{\lambda}_{min} \to -2$ exactly as $\Delta r \to \infty$. In fact, in this limit Eq. (34) reads $\bar{\lambda} \approx 2\cos^4 \alpha \left(5 - 6\cos^2 \alpha\right)$, with minimum at $\alpha = 0$ and a maximum when $\cos^2 \alpha = 5/9$, so that $\bar{\lambda}_{max} = 250/243$, which is one for all practical purposes.

For completeness, we present the total transmitted force $\Lambda = \oint ds\,\bar{\lambda}$ which indicates whether on average the loop is pushing or pulling on the cylinder. It is plotted in Fig. 10(b) in each of the three sequences. Since the p-fold coverings of the equator exert a constant normal force, the initial total force is simply $\Lambda_0 = 2\pi p\,\bar{\lambda}_0$. It if found that Λ tends asymptotically to $\Lambda_\infty \to \pi n$ from below as $\Delta r \to \infty$. Whereas enclosed bound loops both push or pull on the cylinder, depending on the sign of $\bar{\lambda}_0$, ultimately all such loops end up pushing the cylinder.

In the $L_{1,1}$ sequence, the single covering of the equator does not initially exert any force, $\bar{\lambda}_0 = 0$. As Δr increases, however, second order corrections kick in with $\bar{\lambda}$ alternating from positive to negative along the loop. This behavior persists with increasing Δr, see Fig. 5 and the black curves in Fig. 10(a). The negative pulling force on an inner bound loop is increasingly localized in the neighborhood of the tips. We saw earlier that the energy of this state is always higher than that of the planar vertical loop of equal length spanning the interior. Importantly, however, the averaged force is always positive. While the energy would suggest that the $L_{1,1}$ ground state is always unstable, the sign of the contact force suggests otherwise. What appears to occur is that the loop unbinds from the cylinder in the neighborhoods of the tips. If it is short it will rotate into the vertical. As the length increases, however, the lobes pushing on the cylinder snag the loop providing a potential barrier obstructing the passage towards the planar vertical loop. A detailed perturbative study, beyond the scope of this paper, is required to settle the issue.

Along loops in the $L_{1,n}$ sequences, initially $\bar{\lambda}$ is uniformly positive (see Fig. 6(a)) indicating that an Euler type instability is associated with their formation as interior bound states. However this push on the cylinder persists only

---

[12] Recall that this convention is adapted to the viewpoint of an interior loop; if the loops is outside, push and pull are reversed.
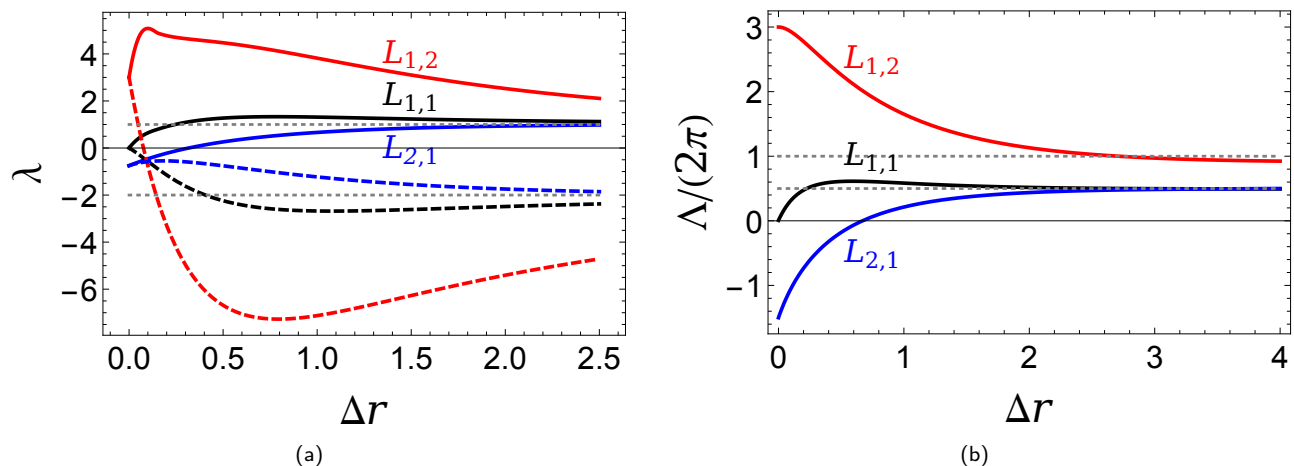
FIG. 10: (Color online) (a) Maximum (solid curves) and minimum (dashed curves) of the magnitude of the normal force λ for sequences $L_{2,1}$ (blue curve), $L_{1,1}$ (black curve) and $L_{1,2}$ (red curve). (b) Total normal force of the same sequences.

for short loops; once $\Delta r > 7.65 \times 10^{-2}$ for $n = 1$ (see the red dashed line in Fig. 10(a)), the minimum of $\bar{\lambda}$ turns negative within the regions near the tips, indicated in Fig. 6(b). In the case of an interior bound state, one would expect the loop to unbind in the neighborhood of its tips so as avoids these regions.

An exterior bound loop with $p = 1$, free to unbind will completely unbind, reforming as a circular loop. As we have already glimpsed, loops in the $L_{2,1}$ sequence behave very differently: now $\bar{\lambda}$ is initially uniformly negative. While an inner bound loop is in this state is manifestly unstable initially, its exterior bound counterpart is stable. However when $\Delta r > 0.317$, the maximum of $\bar{\lambda}$ becomes positive (c.f. the blue solid line in Fig. 10(a)) in the regions surrounding the center of the hairpins, see Fig. 7. Beyond some higher value of Δr the average force becomes positive. This suggests that a sufficiently long interior loop may be stable modulo shortcuts.

As discussed in the perturbative context, doubly-wound exterior loops are more interesting because such loops will always constrict the cylinder. If the loop is short, it will constrict the cylinder everywhere, albeit not in an axially symmetric way. If longer, the contact force will favor the unbinding of the exterior bound loop in the neighborhood of the crossings. However, such loops will remain attached to the cylinder at its hairpins applying a force on the cylinder at the points of contact. In any case the cylinder provides a topological obstruction preventing the doubly wound elastic loop from unraveling into a singly-wound circular loop. This happy conspiracy permitted by the topology has no analogue on a sphere.

V. DISCUSSION AND CONCLUSIONS

We have examined the equilibrium shapes adopted by an elastic loop either confined by a cylinder or constricting it. Our initial motivation was to contrast the behavior of loops confined within a sphere with those confined within a sphere, and specifically to explore how these loops respond to the changed topology. Loops may wind a cylinder any integer number of times. They may oscillate one or more times as they do this. Whereas the winding has no topological significance for a loop that is free to unbind within the cylinder, it very much does if it is bound to the outer surface.

On a sphere, the ground state of a confined loop with a radius exceeding the spherical radius is attached to the sphere. No additional adhesive forces are necessary. The loop pushes against the sphere and it will remain bound everywhere even if free to detach. Instabilities of excited states occur through rearrangements on the sphere itself. When there are topological obstructions, they may be bypassed by stepping into the interior. Elastic loops, however, simply do not bind to the exterior surface of a sphere. What occurs on a cylinder is a lot more interesting.

On a cylinder, one needs to distinguish between stability on the cylinder and off it. We have considered, in detail, the behavior of states bound to the cylinder. If the loop is short there is a single bound ground state for each winding p,

the state with $n = 1$. All states with $n \geq 2$ will be unstable if the loop is short. However, as loops grows in length the sections connecting the troughs and crests straighten out along the axis; if the loop oscillates more than once, the oscillations morph into folded hairpins. All loops grow by extending indefinitely in the axial direction, which permits them to relax their axial torque. One can show that for each $n \geq 2$ there will be a critical length above which the bound folded loop is stabilized. There will be a crossover from instability to stability associated with the exploration of the long (or non-compact) direction. This behavior has no analog on spheres.

If states are free to unbind, the behavior inside and out are very different; both are interesting. Unlike loops binding to spheres, the contact forces are not positive everywhere. Indeed, they are always negative in the neighborhood of the crests and troughs of the oscillations. Interior bound states would be expected to unbind within these regions, lowering the loop curvature and, as a consequence, lowering the loop energy. The ground state itself with $p = 1$, $n = 1$ will also unbind, and if sufficiently short, will be unstable with respect to deformations rotating it off the surface into the confined ground state: a planar loop compressed along its sides. Experimenting with a loop in a cylindrical wastepaper basket or pipe confirms this prediction. Longer partially bound states may become stable beyond some critical length. Folded hairpins will certainly be stable modulo minor adjustments. A stability analysis accommodating normal perturbations is necessary to settle these issues, but it is not going to be simple.

We saw that states with $p > 1$, and $n = 1$ would tend to unbind if below some critical length. This is because the contact forces are inward everywhere. As these states get longer the force turns to push except at the tips so that the state would be expected to stabilize modulo the same sort of corner-cutting we have described. These states are, however, far more interesting placed outside the cylinder.

An exterior loop wrapping a cylinder once will always unbind in the absence of an adhesive force holding it there, reconfiguring itself as a simple circular loop. However, one that wraps the cylinder more than once is constrained by the topology to remain in contact with the cylinder, completely initially and partially–in the neighborhood of its tips–beyond some critical length. In either case it will always apply a compressive force on the cylinder in these neighborhoods. This force generally is not axially symmetric. This behavior can also be confirmed in a broom cupboard experiment by coiling an elastic loop into a figure-of-eight and wrapping a broom handle: whereas a short loop will hug the handle completely, a long one will detach everywhere except at four points. This experiment also reveals that the detached state does not possess the symmetry of its bound counterpart. Indeed, if the loop is coiled three or more times it is clear that the sequence of crossing (over or bellow) is not unique and the detached state will depend on the particular sequence. This mechanism may be relevant to an understanding of the constriction of membrane necks in dynamin mediated membrane vesiculation. It should be remarked that we never anticipated the possibility that loops wrapping a cylinder could bind without any additional agency, never mind, finding that they provide a possible mechanism for neck constriction.

A membrane neck is, of course, better modeled as a catenoid. Modeling the constriction of a catenoid is technically more challenging because along with the surrender of the translational symmetry along the cylinder along its axis one also cedes the quadrature.

An obvious direction for future work is to study open elastic spirals on cylinders, catenoids and other axially symmetric geometries with free boundaries. Spiral geometries represent the behavior of chains of assembled proteins such as dynamin. However, unless physically unrealistic boundary conditions are introduced, the simple elastic energy considered here will not constrict the geometry. A constricting spiral will require an environmental bias, such as a spontaneous normal curvature if it is to apply a force. And if it is to spiral it will require a constraint or bias on the twist which translates into a constraint or bias on the geodesic torsion. This still leaves us with a long way to go before we are in a position to treat a spiral binding to a fluid membrane taking their mutual interaction into account. The consolation is that there is interesting physics to be picked up along the way.

Appendix A: Axisymmetric Surfaces

To describe an axisymmetric surface, it is convenient to introduce cylindrical coordinates (R, φ, Z). adapted to the symmetry with tangent vectors

$$\hat{\boldsymbol{\rho}} = (\cos\varphi, \sin\varphi, 0) \,, \qquad \hat{\boldsymbol{\varphi}} = (-\sin\varphi, \cos\varphi, 0) \,, \qquad \hat{\mathbf{z}} = (0, 0, 1) \,. \tag{A1}$$

The surface is now parametrized by arc-length ℓ along a meridian and the azimuthal angle φ along the parallel:

$$\mathbf{X}(\ell, \varphi) = R(\ell)\hat{\boldsymbol{\rho}} + Z(\ell)\hat{\mathbf{z}} \,, \tag{A2}$$

where $\dot{R}(\ell)^2 + \dot{Z}(\ell)^2 = 1$ and the dot represents derivation with respect to ℓ. The two tangent vectors adapted to this parametrization are

$$\mathbf{e}_\ell = \dot{R}\hat{\boldsymbol{\rho}} + \dot{Z}\hat{\mathbf{z}} \,, \qquad \mathbf{e}_\varphi = R\hat{\boldsymbol{\varphi}} \,. \tag{A3}$$

Thus the line element on the surface is given by $\mathrm{d}s^2 = \mathrm{d}\ell^2 + R(\ell)^2 \, \mathrm{d}\varphi^2$, and the metric tensor assumes the form

$$g_{ab} = \begin{pmatrix} 1 & 0 \\ 0 & R^2 \end{pmatrix} \,. \tag{A4}$$

The outward unit normal vector, $\mathbf{n} = g^{-1/2} \, \mathbf{e}_\varphi \times \mathbf{e}_\ell$ is

$$\mathbf{n} = \dot{Z}\hat{\boldsymbol{\rho}} - \dot{R}\hat{\mathbf{z}} \,; \tag{A5}$$

the extrinsic curvature tensor is diagonal

$$K_{ab} = \begin{pmatrix} -\ddot{R}/\dot{Z} & 0 \\ 0 & R\dot{Z} \end{pmatrix} \,. \tag{A6}$$

The eigenvectors of the shape operator $K^a{}_b = g^{ac} K_{cb}$ (its principal directions) lie along meridians and parallels, with corresponding eigenvalues given by

$$\kappa_\perp = -\ddot{R}/\dot{Z} \,, \qquad \kappa_\parallel = \dot{Z}/R \,. \tag{A7}$$

These are the curvatures of these curves. The two symmetric invariants of the shape operator are the mean and Gaussian curvatures $K = \kappa_\perp + \kappa_\parallel$ and $K_G = \kappa_\perp \, \kappa_\parallel$.

Appendix B: Hamiltonian approach to cylindrical confinement

Here we provide a direct derivation of the "second" integral of the Euler-Lagrange equation describing the confinement of a semi-flexible polymer within a cylinder. The "Lagrangian" density $\mathscr{L}$ is constructed in terms of the three coordinates (φ, z, α)[13] characterizing the curve Γ. These variables are not independent; they are related by Eqs. (12). It will be necessary to implement these constraints using two local Lagrange multipliers λ_φ and λ_z. One thus constructs the following effective energy

$$\mathscr{L}[\alpha, \varphi, z, \alpha', \varphi', z', \lambda_\varphi, \lambda_z] = \int \mathrm{d}s \left(\frac{(\alpha')^2}{2} + \frac{\cos^4 \alpha}{2} + \lambda_\varphi(\varphi' - \cos\alpha) + \lambda_z(z' - \sin\alpha) \right) \,. \tag{B1}$$

The momentum densities conjugate to the coordinates (φ, z, α), are given by

$$P_\varphi = \lambda_\varphi \,, \qquad P_z = \lambda_z \,, \qquad P_\alpha = \alpha' \,. \tag{B2}$$

Since φ and z are cyclic coordinates (because of the rotational and translational symmetries) P_φ and P_z are conserved. Also, L does not depend explicitly on arc-length. Thus its Legendre transformation $\mathcal{H} = \varphi' P_\varphi + z' P_z + \alpha' P_\alpha - \mathcal{L}$ is constant. Evaluating it, one obtains

$$\mathcal{H} = \frac{1}{2} P_\alpha^2 - \frac{\cos^4 \alpha}{2} + P_z \sin\alpha + P_\varphi \cos\alpha \,. \tag{B3}$$

---

[13] As before, here we scale lengths with the cylinder radius

This reproduces the "second" integral Eq. (24) with the identifications, $\mathcal{H} = c$, $f = -P_z$ and $m = -P_\varphi$.

Hamilton's equations for α are

$$\alpha' = \frac{\partial \mathcal{H}}{\partial P_\alpha} = P_\alpha \,, \quad P_\alpha' = -\frac{\partial \mathcal{H}}{\partial \alpha} = -2 \cos^3 \alpha \sin \alpha + P_\varphi \sin \alpha - P_z \cos \alpha \,. \tag{B4}$$

To reconstruct the curve one solves these equations with initial conditions $\alpha(0) = \alpha_0$, $P_\alpha(0) = P_{\alpha 0}$ and fixed P_φ and P_z. The azimuthal and height functions are obtained from integration of the two Hamilton equations

$$\varphi' = \frac{\partial \mathcal{H}}{\partial P_\varphi} = \cos \alpha \,, \quad z' = \frac{\partial \mathcal{H}}{\partial P_z} = \sin \alpha \,. \tag{B5}$$

Without loss of generality one can use the initial conditions $\varphi(0) = 0$ and $z(0) = 0$. The three constants P_z, P_φ and $\mathcal{H}$ are determined from boundary or periodicity conditions.

Appendix C: Confined planar curve

Let us consider the confinement of a closed curve of radius R, lying vertically inside a cylinder of radius R_0, touching the cylinder tangentially on its two sides. We have claimed that this state has lower energy than its bound counterpart. In the absence of additional adhesive forces, the bound interior ground state–if sufficiently short–would be expected to be unstable with respect to deformation into the cylinder rotating it into this state. Since the curve is planar, it is described by the EL equation [18, 20]

$$\varepsilon_{\mathbf{N}} = \kappa'' + \kappa \left(\frac{\kappa^2}{2} - c \right) = 0 \,. \tag{C1}$$

The translational invariance of the bending energy permits one to identify a quadrature

$$(\kappa')^2 + \left(\frac{\kappa^2}{2} - c \right)^2 = F^2 \,, \tag{C2}$$

where F is the magnitude of the force vector $\mathbf{F}$ along the planar curve, given by

$$\mathbf{F} = \left(\frac{\kappa^2}{2} - c \right) \mathbf{T} + \kappa' \mathbf{N} \,. \tag{C3}$$

$\mathbf{F}$ is conserved along the curve, i.e. $\mathbf{F}' = 0$. The quadrature (C2) is integrable in terms of elliptic functions [43, 44]. The specific function will depend on the relative values of F and c [18, 20]:

If $F^2 < c^2$ the FS curvature is given by

$$\kappa(s) = 2 q \, \mathrm{dn}[qs, u] \,, \quad F = u q^2 \,, \quad c = q^2 (2 - u) \,. \tag{C4}$$

where the Jacobi delta function with argument ϕ and parameter u is defined by $\mathrm{dn}^2[\phi, u] = 1 - u \, \mathrm{sn}^2[\phi, u]$ [43]. In one period the curvature will oscillate asymmetrically about the value $\sqrt{2c}$ between two positive (or negative) values, so one has $0 < \kappa_{\min} < \kappa < \kappa_{\max}$, where $\kappa_{\min} = 2 q \sqrt{1 - u}$ and $\kappa_{\max} = 2 q$ ($0 \le u \le 1$, so $F > 0$ and $c > 0$). Thus the curve has an *orbitlike* shape.

If $F^2 = c^2$ the curvature is given by

$$\kappa(s) = 2 q \, \mathrm{sech} \, qs \,, \quad F = c = q^2 \,. \tag{C5}$$

The curve is not periodic, the curvature is positive everywhere but it takes an infinite length for the curve to become planar, that is $\kappa \to 0$ as $s \to \pm \infty$. This curve is termed *borderline* corresponding as it does to the separatrix separating orbital and wavelike behavior.

If $F^2 > c^2$ the curvature is given by

$$\kappa(s) = 2 \sqrt{u} \, q \, \mathrm{cn}[qs, u] \,, \quad F = q^2 \,, \quad c = q^2 (2 u - 1) \,, \tag{C6}$$

where $\mathrm{cn}[\phi, u]$ is the Jacobi cosine elliptic function [43]. The curvature oscillates symmetrically about 0 between $\pm \kappa_M$, i.e. $-\kappa_M < \kappa < \kappa_M$, where $\kappa_M = 2\sqrt{u}\, q$ $(0 \leq u \leq 1)$, so the curve adopts a *wavelike* shape.

The parameters q and u are determined by specifying boundary conditions, which requires knowledge of the embedding functions of the curve.

The cartesian coordinates of the curve $\mathbf{Y} = (x(s), y(s))$ and its tangent vector $\mathbf{T} = (x'(s), y'(s))$ can be expressed in terms of the curvature. Since $\mathbf{F}$ is a constant vector, it is more convenient to work in cartesian coordinates and align it along direction $\hat{\mathbf{x}}$, so $\mathbf{F} = F\,\hat{\mathbf{x}}$, with F constant. Projecting $\mathbf{F}$ onto the cartesian basis $(\hat{\mathbf{x}}, \hat{\mathbf{y}})$, yields

$$x'\left(\frac{\kappa^2}{2} - c\right) - y'\kappa' = F\,, \qquad y'\left(\frac{\kappa^2}{2} - c\right) + x'\kappa' = 0\,. \tag{C7}$$

Taking linear combinations of these equations we get the components of the tangent vector in terms of the curvature and its derivative

$$F\, x' = \frac{\kappa^2}{2} - c\,, \qquad F\, y' = -\kappa'\,. \tag{C8}$$

This can be regarded as a factorization of the quadrature (C2). Introducing the angle ψ that the curve makes with the direction of $\hat{\mathbf{x}}$, the components of the tangent vector can be written as $x' = \cos\psi$ and $y' = \sin\psi$. Also, the curvature is given by the derivative of this angle, $\kappa = \psi'$. Eqs. (C8) can now be mapped into the statement of conservation of energy E and the equation of motion of a pendulum: arclength is identified with time and ψ is identified with the angle that the pendulum makes with the vertical (see, for example, [45]).

Let arclength be measured from the midpoint of the curve, so $x(0) = 0$. Let the contact points occur at an arclength $s = \pm s_b$. The normalized loop length is $l = 4s_b = 2\pi r$, where $r = R/R_0$. Confinement places two constraints on the curve. First, since the curve must align with the container at points of contact, the tangent vector must be vertical at liftoff, therefore $x'(\pm s_b) = 0$ and $y'(\pm s_b) = \mp 1$, thus from Eq. (C8) one has that the constants c and F are given by the curvature and its derivative at the contact points

$$\kappa(\pm s_b) = \sqrt{2c} \quad (c > 0)\,, \qquad \kappa'(\pm s_b) = \pm F\,. \tag{C9}$$

The first condition permits one to obtain the angular wavenumber q in terms of the modulus m. Using expressions (C4), (C5) and (C6) of κ and c in terms of q and u, this condition read for each case

$$qs_b = \mathrm{F}\left[\frac{\pi}{4}, u\right]\,, \qquad\qquad F^2 < c^2\,, \tag{C10a}$$

$$qs_b = \mathrm{arcsinh}\, 1\,, \qquad\qquad F^2 = c^2\,, \tag{C10b}$$

$$qs_b = \mathrm{F}\left[\arcsin\frac{1}{\sqrt{2u}}, u\right] \qquad\qquad F^2 > c^2\,. \tag{C10c}$$

This condition is of an intrinsic character, for it determines the distance of the contact points along the curve. The second condition due to the confinement on the curve is of extrinsic character, for it fixes the spatial distance between the contact points: the coordinates x of the contact points are constrained to be equal to the cylinder radius,

$$x(\pm s_b) = \pm R_0\,. \tag{C11}$$

To implement this constraint one needs to integrate Eqs. (C8). The second equation in (C8) can be integrated readily, which is a consequence of the rotational invariance about the direction orthogonal to the plane of the curve. Indeed, the integration constant is identified as the conserved torque along direction $\hat{\mathbf{z}}$, that is $Fy = -\kappa - M$, where $M = \mathbf{M} \cdot \hat{\mathbf{z}}$. By setting the contact points at $y = 0$, it follows that the magnitude of the torque is given by the negative of the curvature at the contact points, $M = -\kappa_b$. Therefore, the coordinates of the curve are given by

$$x(s) = \frac{1}{F}\int_0^s dt\left(\frac{\kappa(t)^2}{2} - c\right)\,, \qquad y(s) = \frac{1}{F}\left(\kappa_b - \kappa(s)\right)\,. \tag{C12}$$

In full, the cartesian coordinates for each case read

$$x = \frac{2}{u\,q}\,\mathrm{E}[\mathrm{am}[qs,u],u] + \left(1 - \frac{2}{u}\right)s\,, \qquad y = \frac{2}{u\,q}\left(\sqrt{1 - \frac{u}{2}} - \mathrm{dn}[qs,u]\right), \qquad F^2 < c^2\,; \tag{C13a}$$

$$x = \frac{2}{q}\,\tanh qs - s\,, \qquad y = \frac{2}{q}\left(\frac{1}{\sqrt{2}} - \mathrm{sech}\,qs\right), \qquad F^2 = c^2\,; \tag{C13b}$$

$$x = \frac{2}{q}\,\mathrm{E}\left[\mathrm{am}[qs,u],u\right] - s\,, \qquad y = \frac{2}{q}\left(\sqrt{u - \frac{1}{2}} - \sqrt{u}\,\mathrm{cn}[qs,u]\right), \qquad F^2 > c^2\,. \tag{C13c}$$

This segment forms the bottom half of the free loop; the upper half is obtained by an appropriate up-down reflection.

Imposing condition (C11) in Eqs. (C13a) - (C13c) provides another expressions of the wavenumber q in terms of the parameter m, obtaining for each case

$$R_0\,u\,q = 2\,\mathrm{E}\left[\frac{\pi}{4},u\right] - (2 - u)\,\mathrm{F}\left[\frac{\pi}{4},u\right], \qquad F^2 < c^2\,, \tag{C14a}$$

$$R_0\,q = \sqrt{2} - \mathrm{arcsinh}\,1\,, \qquad F^2 = c^2\,, \tag{C14b}$$

$$R_0\,q = 2\,\mathrm{E}\left[\arcsin\frac{1}{\sqrt{2u}},u\right] - \mathrm{F}\left[\arcsin\frac{1}{\sqrt{2u}},u\right] \qquad F^2 > c^2\,. \tag{C14c}$$

By combining Eqs. (C10) and (C14), and using the relation $s_b = \pi\,r/2$ one determines the excess radius $\Delta r = r - 1$ as a function of u

$$\Delta r = \frac{u\,\mathrm{F}\left[\frac{\pi}{4},u\right]}{\pi\left(\mathrm{E}\left[\frac{\pi}{4},u\right] - \left(1 - \frac{u}{2}\right)\mathrm{F}\left[\frac{\pi}{4},u\right]\right)} - 1\,, \qquad F^2 < c^2\,, \tag{C15a}$$

$$\Delta r = \frac{2\,\mathrm{arcsinh}\,1}{\pi\left(\sqrt{2} - \mathrm{arcsinh}\,1\right)} - 1\,, \qquad F^2 = c^2\,, \tag{C15b}$$

$$\Delta r = \frac{\mathrm{F}\left[\arcsin\frac{1}{\sqrt{2u}},u\right]}{\pi\left(\mathrm{E}\left[\arcsin\frac{1}{\sqrt{2u}},u\right] - \frac{1}{2}\mathrm{F}\left[\arcsin\frac{1}{\sqrt{2u}},u\right]\right)} - 1\,, \qquad F^2 > c^2\,. \tag{C15c}$$

This makes it possible to parametrize the loop by u. Alternatively one can solve Eqs. (C15) numerically in each case to determine u for a given excess radius Δr.

The total energy of the loop is easily obtained by noticing from Eq. (C8) that the energy density is proportional to x'. Thus, the energy of one quarter of the loop is given by

$$\frac{H_B}{4} = \frac{1}{2}\int_0^{s_b} \mathrm{d}s\,\kappa^2 = \int_0^{s_b} \mathrm{d}s\,(F\,x' + c) = F\,R_0 + c\,s_b\,, \tag{C16}$$

which establishes the role of the constants F and c as the conjugate variables to the extrinsic and intrinsic lengths of the curve respectively (cf. Eq. (32) for the confined case). Using Eqs. (C10) and (C14), one gets that the total energy of the loop in each of the three cases by

$$H_B = 8\,q\,\mathrm{E}\left[\frac{\pi}{4},u\right], \qquad F^2 < c^2\,, \tag{C17a}$$

$$H_B = 4\sqrt{2}\,q\,, \qquad F^2 = c^2\,, \tag{C17b}$$

$$H_B = 8\,q\left(\mathrm{E}\left[\arcsin\frac{1}{\sqrt{2u}},u\right] - (1 - u)\,\mathrm{F}\left[\arcsin\frac{1}{\sqrt{2u}},u\right]\right), \qquad F^2 > c^2\,. \tag{C17c}$$

One quarter of the confined loops are plotted for increasing radius in Fig. 11(a). If $u = 0$ one has a circle. In the range $0 < \Delta r < 0.053$ ($0 < u < 1$) the curve is consists of orbitlike elastica segments, whereas for $\gamma > 0.053$ ($1/2 < u < 1$, u decreases as the length increases) it consists of wavelike elastica segments (at $\Delta r = 0.053$ ($u = 1$) consists of borderline elastica segments). In this wavelike regime, when $\Delta r = 0.393$ ($u = 1/2$) the curve adopts the limit shape shown in Fig. 11(a) and by further increasing the length, the middle region of the loop–where the curve makes contact with

the cylinder–will elongate, so the two limit arcs will be separated by straight lines. The energy of the loops is plotted in Fig. 11(b) as a function of their radius. The bending energy H_B of the confined loops begins at $H_B/\pi = 1/R_0$ (circle with $u = 0$) and decreases monotonically as the radius of the loop increases, saturating when the limit shape with straight segments is reached for such lines do not contribute to the bending energy.[14] The normal force acting
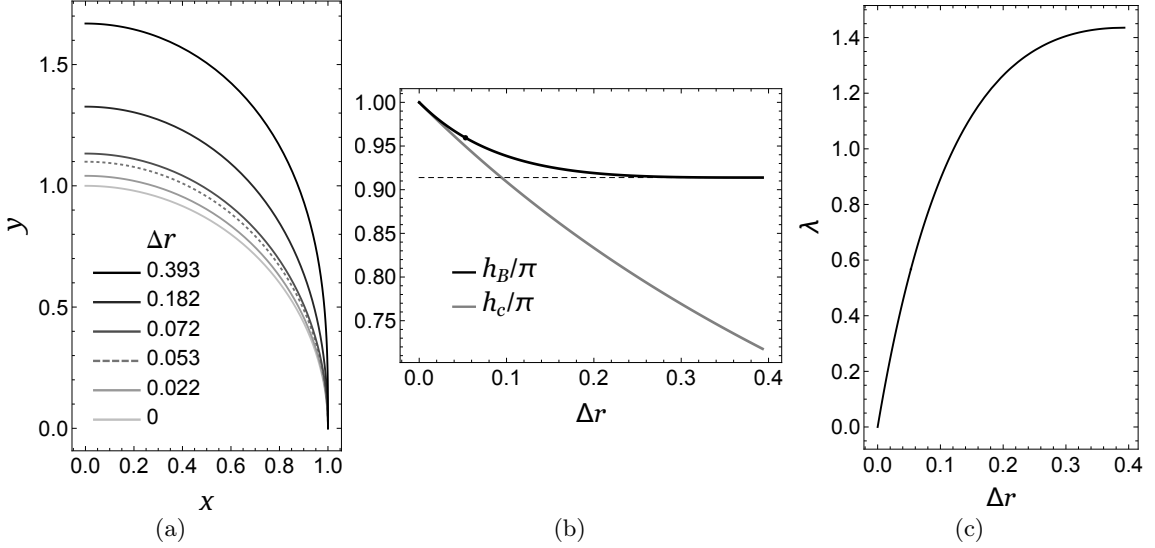

FIG. 11: (a) One quarter of vertical elastic loops of different radii R confined inside a cylinder of R_0 ($\Delta r = R/R_0 - 1$). The loops have vertical tangent at two points where they touch the cylinder. The shortest curve is the circle with radius equal to the cylinder ($\Delta r = 0$). In the interval $0 < \Delta r < 0.053$ the loop is composed by arcs of orbitlike elasticas (light gray curve), when $\Delta r = 0.053$ of a segment of the borderline elastica (dashed curve) and after which is formed by wavelike elastica segments (dark gray curves), reaching a limit shape at $\Delta r = 0.393$ (black curve), such that beyond this point the excess length will located at the contact regions, so the vertical intermediate region will increase. (b) Bending energy of the confined loops as a function of their reduced radius. The black dot represent the energy of the loop formed by borderline elastica segments, curves with smaller (greater) radius consist of orbitlike (wavelike) elasticas. H_B starts at value of π/R_0 and decreases monotonically (black curve)–but much slower than the bending energy of a free loop (gray line)– as the loop radius increases, reaching a limit value of $0.914\,\pi$ for the curve with $\Delta r = 0.393$, after which it remains constant, regardless of the loop length. (c) Magnitude of the normal force transmitted to the cylinder at the points where contact is made.

on the point where contact with the cylinder occurs is given by $\lambda = 2\,F$ (each arc contributes with an amount F). This can be seen by considering a stress source of magnitude λ acting on the point of contact at $s = s_b$, in the EL equation (C1)

$$\varepsilon_{\mathbf{N}} = \kappa'' + \kappa\left(\frac{\kappa^2}{2} - c\right) = \lambda\,\delta(s - s_b)\,. \tag{C18}$$

Integrating this equation in the neighborhood of the contact point and taking into account that the curvature is continuous across the contact region,[15] one has

$$\int_{s_b - \delta s}^{s_b + \delta s} \mathrm{d}s\,\varepsilon_{\mathbf{N}} = \kappa'_+ - \kappa'_- = \lambda\,. \tag{C19}$$

where κ'_+ and κ'_- are the limits of the arclength derivative of the curvature, on the top and bottom sides of the contact point. Thus the force exerted on the loop is reflected by the discontinuity in the derivative of its curvature. This is analogous to the force exerted on a fluid vesicle by a ring, presented in Ref. [28]. From the BCs. (C9), one has $\kappa'_\pm = \pm F$, so $\lambda = 2F$.[16] Moreover, from Eqs. (C4)-(C6) follows that λ is proportional to the squared wavenumber,

---

[14] This decay is slower than that of the energy in a free loop $H_{B0} = \pi/R$, and achieves a limit value rather than tending to zero for very long loops.

[15] If an adhesion energy is considered, the curvature would have a discontinuity [46, 47]

[16] The change of sign between the up and down regions stems from the fact that it is obtained by a reflection of the top arc, rather than a periodic continuation of the corresponding elastica.

which is plotted in Fig. 11(c). As the loop radius increases, λ increases from 0 (circle) to a constant value 1.435 (limit arc). When the straight lines appear, they do not exert a force on the cylinder and the corresponding normal force for each arc $\lambda = F$ is non vanishing only at the points of detachment.

Appendix D: Closed curves with zero axial force and torque

Loops of special interest are those in which not only the axial force vanishes but, in addition, the axial torque vanishes, i.e. $m = 0$.[17] While this condition is met in infinitely long loops, rather surprisingly it is also met non-trivially for loops of specific length and precise values of n and p. Now the constant c given in Eq. (60) simplifies to $c = -\cos^4_M/2 = \bar{\kappa}^2_{n\,M}/2$, so the quadrature (24) reduces to $\alpha'^2 = \cos^4\alpha - \cos^4\alpha_M$, which can be recast in terms of the scaled normal curvature as

$$\bar{\kappa}'_n = 2\sqrt{\bar{\kappa}_n\,(1 - \bar{\kappa}_n)\,(\bar{\kappa}^2_n - \bar{\kappa}^2_{nM})}\,. \tag{D1}$$

Solutions exist in the range $0 \leq \bar{\kappa}_{nM} \leq \bar{\kappa}_n \leq 1$, so that the normal curvature will oscillate between a mimimum $\bar{\kappa}_{nM} \in (0,1)$ at points where the loop crosses the equator ($\alpha = \alpha_M$) and 1 at points with minimum and maximum height ($\alpha = 0$). One finds an exact analytic solution upon integrating Eq. (D1)

$$s = \frac{1}{\sqrt{2\,\bar{\kappa}_{nM}}}\,\mathrm{F}\left[\arcsin\sqrt{\frac{1 - \bar{\kappa}_n}{1 - \bar{\kappa}_{nM}}\,\frac{2\bar{\kappa}_{nM}}{\bar{\kappa}_n + \bar{\kappa}_{nM}}}\,, \frac{1 - \bar{\kappa}_{nM}}{2}\right]\,, \tag{D2}$$

where $\mathrm{F}[u, m]$ is the elliptic function of the first kind. Here arc-length s is measured from the tips where $\kappa_n = 1$. The arc-length measured from tip to crossing point is given by $s_M = \mathrm{K}[(1 - \bar{\kappa}_{nM})/2]/\sqrt{2\,\bar{\kappa}_{nM}}$, so that the total length of the loop is $l = 4ns_M$ and the excess radius is $\Delta r = 2ns_M/\pi - p$.

The normal curvature as a function of arc-length is identified by inverting (D2)

$$\bar{\kappa}_n(s) = \frac{\bar{\kappa}_{nM}\,\mathrm{dn}^2\left[\sqrt{2\,\bar{\kappa}_{nM}}\,s, (1 - \bar{\kappa}_{nM})/2\right]}{1 + \bar{\kappa}_{nM} - \mathrm{dn}^2\left[\sqrt{2\,\bar{\kappa}_{nM}}\,s, (1 - \bar{\kappa}_{nM})/2\right]}\,, \tag{D3}$$

where $\mathrm{dn}[u, m]$ is the Jacobi delta function. Both the height and azimuthal functions can be determined by combining the quadrature (D1) with the relations $\varphi' = \cos\alpha = \sqrt{\bar{\kappa}_n}$ and $z' = \sin\alpha = \sqrt{1 - \bar{\kappa}_n}$ and integrating:

$$\varphi(s) = \frac{1}{\sqrt{1 + \bar{\kappa}_{nM}}}\,\mathrm{F}\left[\arcsin\sqrt{\frac{1 - \bar{\kappa}_n(s)}{1 - \bar{\kappa}_{nM}}}\,, \frac{1 - \bar{\kappa}_{nM}}{1 + \bar{\kappa}_{nM}}\right]\,, \tag{D4a}$$

$$z(s) = \frac{1}{\sqrt{2\,\bar{\kappa}_{nM}}}\left(\mathrm{K}\left[\frac{1}{2}\right] - \mathrm{F}\left[\arcsin\sqrt{\frac{2\,\bar{\kappa}_{nM}}{\bar{\kappa}_n(s) + \bar{\kappa}_{nM}}}\,, \frac{1}{2}\right]\right)\,. \tag{D4b}$$

The maximum height $z_{\max}$ occurs at the tips where $\bar{\kappa}_n = 1$. The total azimuthal extension of the loops is

$$\Delta\varphi = \frac{4\,n}{\sqrt{1 + \bar{\kappa}_{nM}}}\,\mathrm{K}\left[\frac{1 - \bar{\kappa}_{nM}}{1 + \bar{\kappa}_{nM}}\right]\,. \tag{D5}$$

Closure $\Delta\varphi = 2\pi p$ implies that the corresponding wave number is given by

$$q = \frac{n}{p} = \frac{\pi}{2}\,\sqrt{1 + \bar{\kappa}_{nM}}/\mathrm{K}\left[\frac{1 - \bar{\kappa}_{nM}}{1 + \bar{\kappa}_{nM}}\right]\,. \tag{D6}$$

In Fig. 12 q is plotted as a function of $\bar{\kappa}_{nM}$. We see that the wavenumber is bounded in the interval $0 < q < \sqrt{2}$. Excited states with vanishing torque do not exist in any sequence with $p = 1$; the only such state is an elliptic ground state with $n = 1$ and $m = 0$ (cf Fig. 3). For a given q one has to solve numerically Eq. (D6) to determine $\bar{\kappa}_{nM}$.

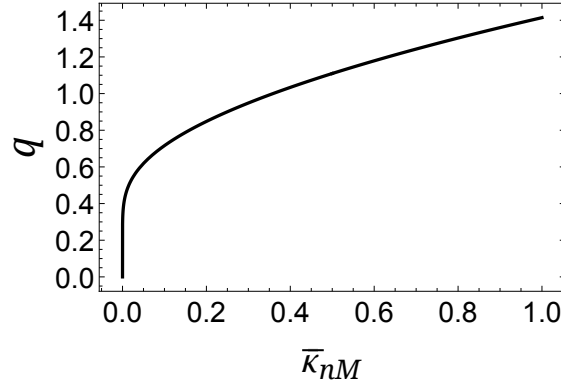[17] Note, of course, that the total non-conserved, torque does not vanish in these states.

FIG. 12: Allowed wavenumbers for loops with zero axial torque and force. The loops are defined for wavenumbers given by rational numbers in the range $0 < n/p < \sqrt{2}$.
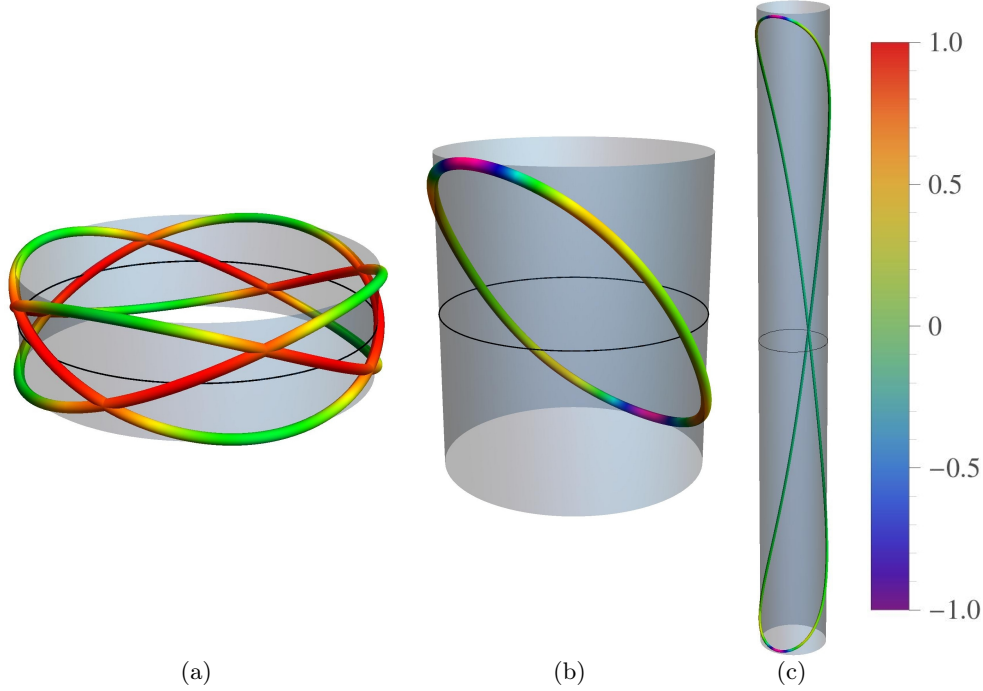

(a) (b) (c)

FIG. 13: (Color online) Curves with zero axial force and torque with (a) $p = 3$, $n = 4$ and $\Delta r = 0.122$ ($\alpha_M = 0.125\,\pi$); (b) $p = 1$, $n = 1$ and $\Delta r = 0.297$ ($\alpha_M = 0.296\pi$); (c) $p = 2$, $n = 1$ and $\Delta r = 4.8$ ($\alpha_M = 0.461\pi$). The normalized magnitude of the normal force λ is color-coded in these figures.

Loops with $q = 4/3, 1$ and $1/2$ are illustrated in Fig. 13. Their corresponding scaled normal curvatures at the crossing points are $\bar{\kappa}_{nM} = 0.853, 0.359$ and 0.015 respectively.

Loops with $\bar{\kappa}_{nM} \approx 1$ will be close to p-coverings of the equator. As $\bar{\kappa}_{nM}$ decreases towards zero the loops elevate, getting more and more vertical as $\bar{\kappa}_{nM}$ tends to zero. In the limit case $\bar{\kappa}_{nM} = 0$, the reduced normal curvature and the coordinate functions assume a simple form. For $c = 0$, the quadrature reduces to $\alpha' = \cos^2 \alpha$, so $\tan \alpha = s$ and $\bar{\kappa}_n = 1/(s^2 + 1)$, whereas the azimuthal and height coordinates for this case can be represented by $\varphi = \text{arcsinh}\, s$ and $z = \sqrt{s_M^2 + 1} - \sqrt{s^2 + 1}$, which together permits one to express the normal curvature and the height in terms of azimuthal angle as $\bar{\kappa}_n = \text{sech}^2\varphi$ and $z = \cosh\varphi_M - \cosh\varphi$. Thus it takes an infinite number of windings and infinite height to go from the tips with $\bar{\kappa}_n = 1$ ($\varphi = 0$) to the points crossing the equator with $\bar{\kappa}_n = 0$ ($\varphi \to \infty$), where the loops have vertical tangents. Therefore the loop has infinite excess radius and winds infinitely many times while completing one period, so $n = 1$ and $p \to \infty$, and consequently $q = 0$.

The energy of a curve with length $l = 2\,s_b$ is given by

$$h_B = 4\,n \int_0^{s_M} \mathrm{d}s\, \bar{\kappa}_n^2 - \bar{\kappa}_{nM}^2\, l/2\,. \tag{D7}$$

There is no analytic expression in terms of elliptic functions, so it has to be integrated numerically. The energy of the limit loop with $\bar{\kappa}_{nM} = 0$ is $h_b = \pi$, $(n = 1)$.

The magnitude of the normal force is given by

$$\bar{\lambda}(s) = 2\,\bar{\kappa}_n^2(s)\,(5 - 6\,\bar{\kappa}_n(s)) + 3\,\bar{\kappa}_{nM}^2\,(2\,\bar{\kappa}_n(s) - 1)\,. \tag{D8}$$

For the limit loop with $\bar{\kappa}_{nM} = 0$, the magnitude of the normal force can be parametrized by the azimuthal angle as $\bar{\lambda} = 2\,\mathrm{sech}^4\,\varphi\,(5 - 6\,\mathrm{sech}^2\,\varphi)$. It vanishes as $\varphi \to \infty$, which corresponds to the points crossing the equator.

Appendix E: Comparison of cylindrical and planar elastic curves

To visualize the development of overhangs and the subsequent self-intersection of the loops as the length is increased, it is useful exploit the isometry between the cylinder and the plane. This is achieved by cutting the cylinder along the meridian passing through the lower turning point along the loop and "unrolling" it, as indicated in Fig. 14. If $\alpha_M \le \pi/2$, the azimuthal extension of the loop on either side of the equator is bounded by π ($\Delta\varphi_{max} \le \pi$). See Figs. 14 (a)-(d).[18] Overhangs (with $\varphi' = 0$), signaling the appearance of lobes, first appear on the equator. If $\alpha_M > \pi/2$, then $\Delta\varphi_{max} > \pi$, and the loop necessarily develops overhangs. See Fig. 14(e). The azimuthal extension grows monotonically with length: at some point $\Delta\varphi_{max} = 2\pi$ and the loop makes self contact for the first time. See Fig. 14(f). As the length is increased further, the overhangs grow indefinitely; overlapping repeatedly as they wrap the cylinder.

It is also useful to compare loops on the cylinder with the corresponding planar Euler-elastic curves (dashed gray curves) of the same length passing through the same two points on the unrolled equator. These are superimposed on the unrolled loops in Fig. 14. Initially the cylindrical loop behaves like a planar elastic curve (Figs. 14(a)-(b)). As the length is increased, however, the term in the potential quadratic in the normal curvature begins to play a role and the behavior of the two diverges, as indicated in Figs. 14(c)-(d). In a long loop, this term dominates: its effect is to elongate the cylindrical loop along the axial direction. This contrasts with its rounded planar counterpart which distributes its curvature equally in azimuthal and vertical directions. See 14(e)-(f). The corresponding evolutions of the L_{12} and L_{21} are presented in Figs. 15 and 16. For the latter sequence, the cut is made at the point of self-intersection on the equator. In Fig. 16(f) one can see that loops with obtuse angles extend over a azimuthal range $> 2\pi$ (the vertical dotted gray lines).

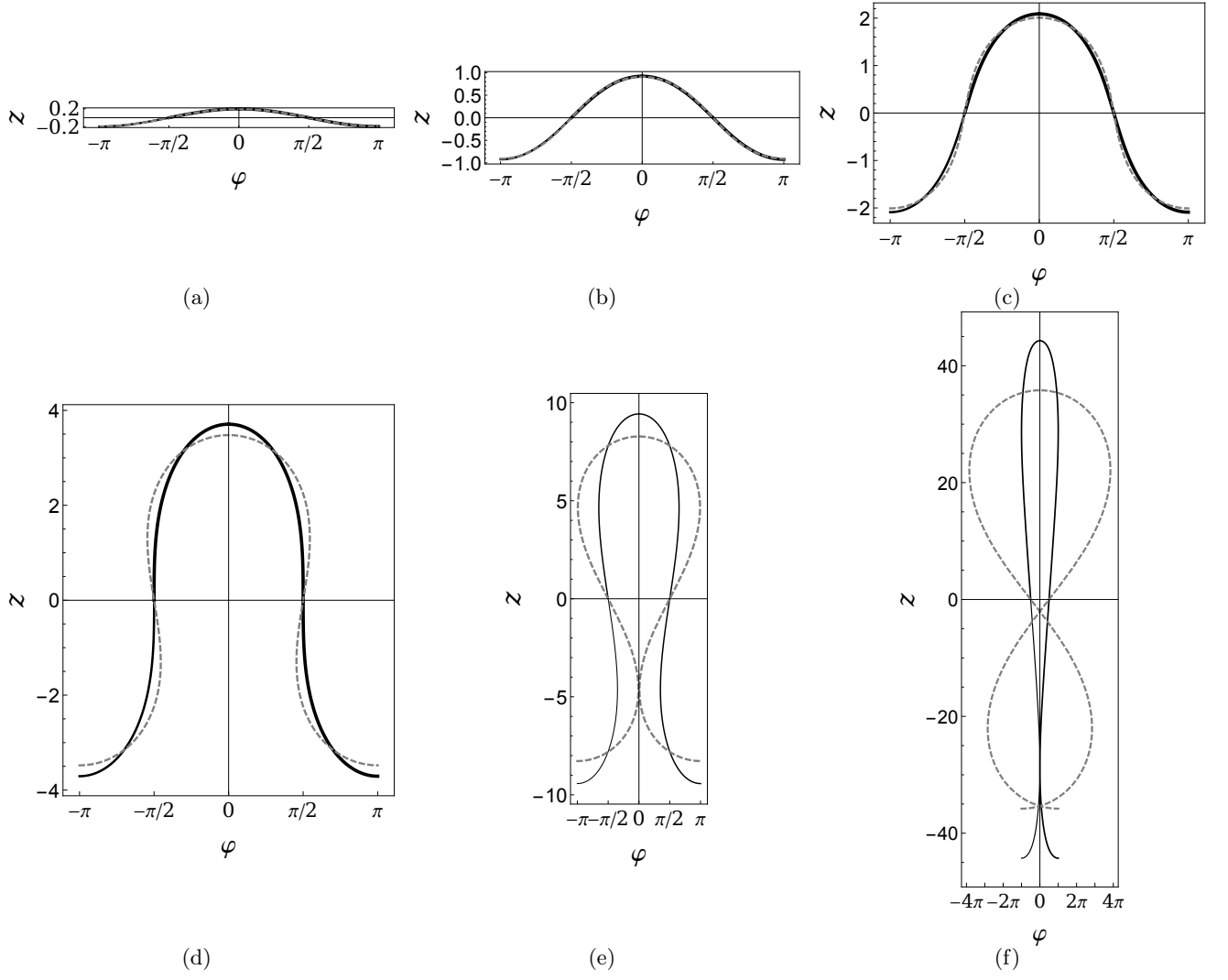[18] The intersections of the loop with the equator are always separated by π.

31

FIG. 14: Unfolding loops in the $L_{1,1}$ sequence illustrated in Fig. 5 are represented by black solid curves, whereas their planar Euler-elastic counterparts (equal length and same midpoints) are represented by gray dashed curves. For small excess radius the two coincide, but they differ increasingly as the excess radius grows.
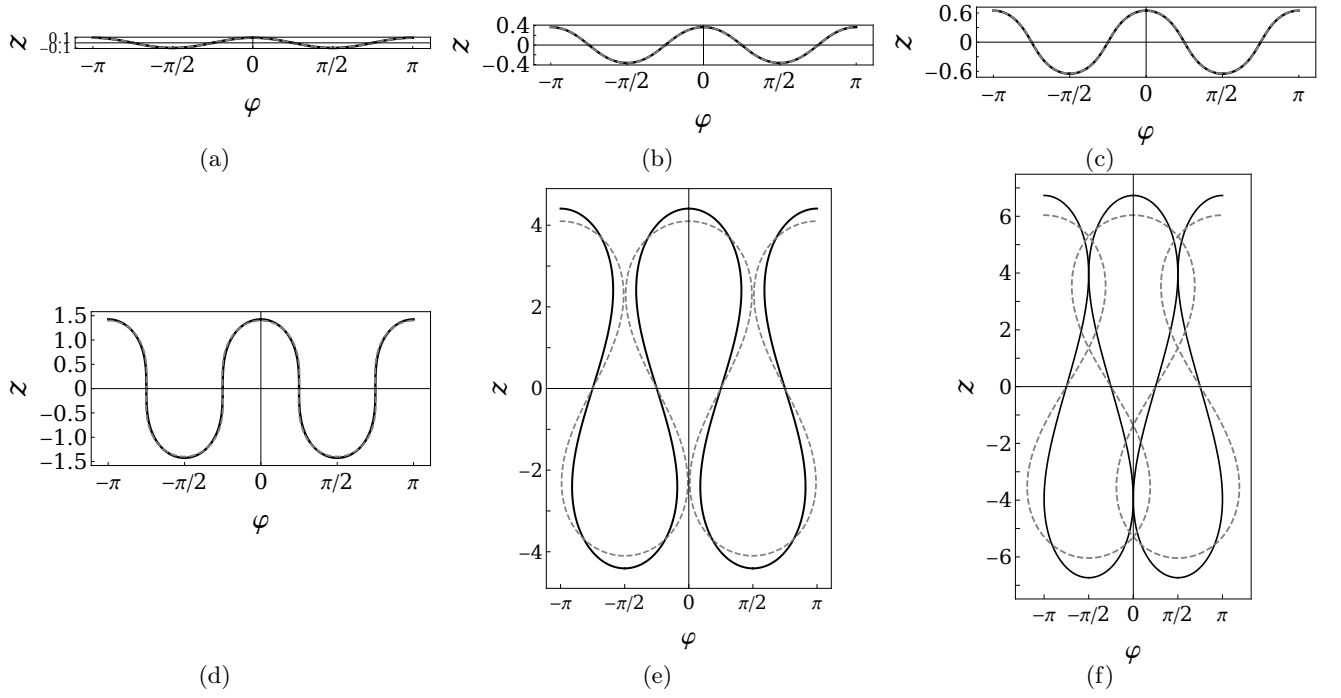
(a) (b) (c)

(d) (e) (f)

FIG. 15: Unfolding loops in the $L_{1,2}$ sequence illustrated in Fig. 6 are indicated by solid black curves. Their planar counterparts (equal length and same midpoints) are indicated by gray dashed curves. In contrast to the $L_{1,1}$ sequence, the two agree pretty well even when the length is significant.
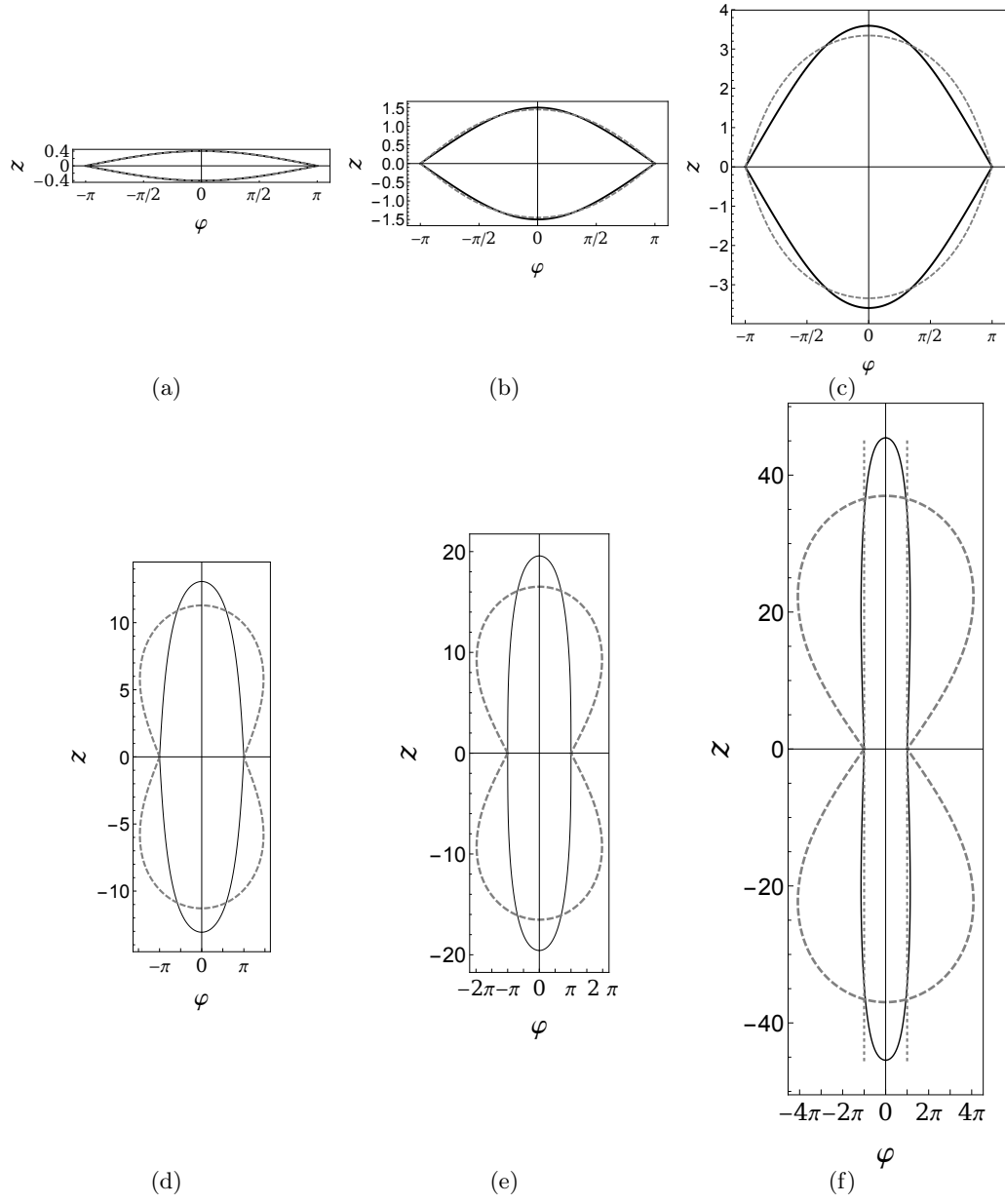
FIG. 16: Unfolded version of loops of sequence $L_{2,1}$ illustrated in Fig. 7 are represented by black solid curves, whereas the planar Euler-elasticas with the same length and same midpoints are represented by gray dashed curves.

[1] J. F. Marko and E. D. Siggia, Macromolecules **28**, 8759 (1995).
[2] A. Ott, M. Magnasco, A. Simon, and A. Libchaber, Phys. Rev. E **48**, R1642 (1993).
[3] F. Gittes, B. Mickey, J. Nettleton, and J. Howard, The Journal of Cell Biology **120**, 923 (1993).
[4] K. Luger, A. W. Mader, R. K. Richmond, D. F. Sargent, and T. J. Richmond, Nature **389**, 251 (1997).
[5] H. Schiessel, Journal of Physics: Condensed Matter **15**, R699 (2003).
[6] A. G. Cherstvy and V. B. Teif, Physical Biology **11**, 044001 (2014).
[7] D. Discher, N. Mohandas, and E. Evans, Science **266**, 1032 (1994).
[8] T. Dechat, K. Pfleghaar, K. Sengupta, T. Shimi, D. K. Shumaker, L. Solimando, and R. D. Goldman, Genes & Development **22**, 832 (2008).
[9] K. N. Dahl, A. J. Ribeiro, and J. Lammerding, Circulation Research **102**, 1307 (2008).
[10] S. Morlot and A. Roux, Annual Review of Biophysics **42**, 629 (2013).
[11] M. M. Kozlov, Traffic **2**, 51 (2001).
[12] J. E. Hinshaw and S. L. Schmid, Nature **374**, 190 (1994).
[13] P.-G. de Gennes, in *Polymers in Confined Environments*, Advances in Polymer Science, Vol. 138, edited by S. Granick, K. Binder, P.-G. de Gennes, E. Giannelis, G. Grest, H. Hervet, R. Krishnamoorti, L. Léger, E. Manias, E. Raphaël, and S.-Q. Wang (Springer Berlin Heidelberg, 1999) pp. 91–105.
[14] N. Fakhri, D. A. Tsyboulski, L. Cognet, R. B. Weisman, and M. Pasquali, Proceedings of the National Academy of Sciences **106**, 14219 (2009).
[15] E. T. Thostenson, Z. Ren, and T.-W. Chou, Composites Science and Technology **61**, 1899 (2001).
[16] L. Wei and L. C. M., Nat Mater **6**, 841 (2007).
[17] O. Kratky and G. Porod, Recueil des Travaux Chimiques des Pays-Bas **68**, 1106 (1949).
[18] J. Langer and D. A. Singer, Journal of Differential Geometry **20**, 1 (1984).
[19] J. Kierfeld, K. Baczynski, P. Gutjahr, and R. Lipowsky, AIP Conference Proceedings **1002**, 151 (2008).
[20] D. A. Singer, AIP Conference Proceedings **1002**, 3 (2008).
[21] A. E. H. Love, *A Treatise on the Mathematical Theory of Elasticity*, 4th ed. (Cambridge University Press, New York, 2013).
[22] S. Antman, *Nonlinear Problems of Elasticity*, 2nd ed. (Springer, Dordrecht, 2005).
[23] L. Landau, L. P. Pitaevskii, A. M. Kosevich, and E. Lifshitz, *Theory of Elasticity*, 3rd ed., Vol. 7 (Butterworth-Heinemann, Oxford, 1986).
[24] B. Audoly and Y. Pomeau, *Elasticity and geometry: from hair curls to the non-linear response of shells* (Oxford Univ. Press, New York, NY, 2010).
[25] R. Capovilla, C. Chryssomalakos, and J. Guven, Journal of Physics A: Mathematical and General **35**, 6571 (2002).
[26] J. Guven, D. M. Valencia, and P. Vázquez-Montejo, Journal of Physics A: Mathematical and Theoretical **47**, 355201 (2014).
[27] J. Guven and P. Vázquez-Montejo, Phys. Rev. E **85**, 026603 (2012).
[28] B. Božič, J. Guven, P. Vázquez-Montejo, and S. Svetina, Phys. Rev. E **89**, 052701 (2014).
[29] G. S. Manning, Quart. Appl. Math. **45**, 515 (1987).
[30] H. K. Nickerson and G. Manning, Geometriae Dedicata **27**, 127 (1988).
[31] N. L. Marky and G. S. Manning, Biopolymers **31**, 1543 (1991).
[32] G. H. M. van der Heijden, Proceedings of the Royal Society of London A: Mathematical, Physical and Engineering Sciences **457**, 695 (2001).
[33] G. H. M. van der Heijden, A. Champneys, and J. M. T. Thompson, International Journal of Solids and Structures **39**, 1863 (2002).
[34] G. H. M. van der Heijden, M. Peletier, and R. Planqué, Archive for Rational Mechanics and Analysis **182**, 471 (2006).
[35] N. Stoop, J. Najafi, F. K. Wittel, M. Habibi, and H. J. Herrmann, Phys. Rev. Lett. **106**, 214102 (2011).
[36] J. Najafi, N. Stoop, F. Wittel, and M. Habibi, Phys. Rev. E **85**, 061108 (2012).
[37] J. Shin, A. G. Cherstvy, and R. Metzler, New Journal of Physics **16**, 053047 (2014).
[38] J. Shin, A. G. Cherstvy, and R. Metzler, ACS Macro Letters **4**, 202 (2015).
[39] A. G. Cherstvy, The Journal of Physical Chemistry B **115**, 4286 (2011).
[40] S. J. de Carvalho, R. Metzler, and A. G. Cherstvy, arXiv preprint arXiv:1503.02040 (2015).
[41] E. Kreyszig, *Differential Geometry* (Dover Publications, New York, 1991).
[42] J. Guven, M. M. Müller, and P. Vázquez-Montejo, Journal of Physics A: Mathematical and Theoretical **45**, 015203 (2012).
[43] M. Abramowitz and I. Stegun, *Handbook of Mathematical Functions, With Formulas, Graphs, and Mathematical Tables* (Dover Publications, 1974).
[44] I. Gradshteyn and I. Ryzhik, *Table of Integrals, Series, and Products*, edited by A. Jeffrey and D. Zwillinger (Elsevier Academic Press, Boston, 2007).
[45] P. A. Djondjorov, M. T. Hadzhilazova, I. M. Mladenov, and V. M. Vassilev, in *Ninth International Conference on Geometry, integrability and quantization*, Vol. 9, edited by I. M. Mladenov (SOFTEX, Sofia, 2008) pp. 175–186.
[46] M. Deserno, M. M. Müller, and J. Guven, Phys. Rev. E **76**, 011605 (2007).
[47] U. Seifert and R. Lipowsky, Phys. Rev. A **42**, 4768 (1990).